Wiley Analytical Science

Virtual Conference

The 5th edition of the Wiley Analytical Science Conference starts November 8, 2022!

Featured Sessions:

- **Integration of X-ray microscopy and finite elements into a digital twin**

  Thurs Nov 10, 10:00 - 10:30 AM EST / 4:00 - 4:30 PM CET

- **Optimization of Cryo TEM lamella preparation workflows to be faster and more accessible**

  Wed Nov 16, 10:00 - 11:00 AM EST / 4:00 - 5:00 PM CET

events.bizzabo.com/WASconferenceFall2022

ZEISS
Seeing beyond

TESCAN
PERFORMANCE IN NANOSPACE

WILEY

Organic Neuroelectronics: From Neural Interfaces to Neuroprosthetics

Gyeong-Tak Go, Yeongjun Lee, Dae-Gyo Seo, and Tae-Woo Lee*

Requirements and recent advances in research on organic neuroelectronics are outlined herein. Neuroelectronics such as neural interfaces and neuroprosthetics provide a promising approach to diagnose and treat neurological diseases. However, the current neural interfaces are rigid and not biocompatible, so they induce an immune response and deterioration of neural signal transmission. Organic materials are promising candidates for neural interfaces, due to their mechanical softness, excellent electrochemical properties, and biocompatibility. Also, organic nervetronics, which mimics functional properties of the biological nerve system, is being developed to overcome the limitations of the complex and energy-consuming conventional neuroprosthetics that limit long-term implantation and daily-life usage. Examples of organic materials for neural interfaces and neural signal recordings are reviewed, recent advances of organic nervetronics that use organic artificial synapses are highlighted, and then further requirements for neuroprosthetics are discussed. Finally, the future challenges that must be overcome to achieve ideal organic neuroelectronics for next-generation neuroprosthetics are discussed.

1. Introduction

Neuroelectronics has applications for diagnosis and treatment of neurological diseases by transmitting physiological signals between physically and electrically interfaced tissues. Neural

G.-T. Go, D.-G. Seo, T.-W. Lee
Department of Materials Science and Engineering
Seoul National University
1 Gwanak-ro, Gwanak-gu, Seoul 08826, Republic of Korea
E-mail: twlees@snu.ac.kr
Y. Lee
Department of Chemical Engineering
Stanford University
Stanford, CA 94305, USA
T.-W. Lee
Institute of Engineering Research
Research Institute of Advanced Materials
Soft Foundry
Seoul National University
1 Gwanak-ro, Gwanak-gu, Seoul 08826, Republic of Korea
T.-W. Lee
School of Chemical and Biological Engineering
Seoul National University
1 Gwanak-ro, Gwanak-gu, Seoul 08826, Republic of Korea

The ORCID identification number(s) for the author(s) of this article can be found under https://doi.org/10.1002/adma.202201864.

signals transmit various information from internal and external environments of organisms to each organ. Neurological diseases can impede transmission of neural signals and can cause severe symptoms. These diseases significantly reduce the quality of life, and can also be life-threatening. Neurological disease is a leading cause of disability-adjusted life-years (DALYs) which affected more than 276 million people globally in 2016.[1] In 2010 in the US, DALYs of spinal cord injuries were 445 911, which was higher than those of human immunodeficiency virus (HIV)/acquired immune deficiency syndrome (AIDS).[2] Drugs and neurosurgery are being developed to treat neurological diseases, but due to complex pathophysiology are not always effective.[3] Cell therapies repair the damaged tissues by introducing new cells, and gene therapies treat neurological disease by introducing genes into the body. These therapies enable fundamental treatment because they remove damaged cells and defective genes that are the causes of the diseases, but may cause severe or fatal side-effects such as immune responses.[4,5] Therefore, new methods for general treatment of neurological disease are being sought.

Electric therapy is a promising method to diagnose disease by recording neural electronic signals and to treat disorders by using electrical signals to stimulate tissues.[6] The electrical stimulation has few side-effects, and is regarded as a possible and safe method to treat intractable neurological disorders.[7] For example, electrical stimulation has successfully recovered the lost functions from spinal cord injury.[8] However, despite these advantages, the development of neuroelectronics is still in its infancy; further research must be conducted to improve its efficacy and stability and to ensure that it does not limit daily life.

Neuroelectronics can be divided into two main categories: neural interfaces that record or stimulate neural signals, and neuroprosthetics that replace damaged sensory and motor organs and neural signal pathway. Among the diverse forms of neuroprosthetics, this review focuses on bioelectronic devices that relay electrophysiological signals by bypassing damaged nerves. Conventionally, metal electrodes have been developed as a neural electrode for diagnosis and treatment due to their high electrical conductivity, and ease of processing in high density arrays.[9–11] For example, use of metal electrodes for electroencephalography (EEG) is a promising method to diagnose epilepsy.[12] Also, deep

**ADVANCED
SCIENCE NEWS**

www.advancedsciencenews.com

**ADVANCED
MATERIALS**

www.advmat.de

brain stimulation (DBS) using metallic intracranial electrodes is an effective method to treat Parkinson's disease.[13,14] Flexible metallic microelectrode arrays (MEAs) have been miniaturized to subcellular feature size with tissue-level flexibility, and have demonstrated long-term reliable neural integration by avoiding the glial scar formation and neuronal degradation that can occur when rigid metallic MEAs are used.[15,16] However, the metal interfaces have disadvantages such as high stiffness, low electrochemical capacity, and poor tissue interaction.[17,18] To replace conventional metallic neural electrodes, novel materials and device structure must be developed.

Conventionally neuroprosthetics use complementary metal–oxide–semiconductor (CMOS) chips and circuits to process neural signals recorded from the biological nervous systems.[19] For example, the electrical implants record action potentials at one location in the brain and deliver the electrical stimuli to another location in the brain.[19,20] As a result, a new synthetic connection is established between two previously independent sites; this modification has been achieved in the brains of rodents and primates as well.[19,20]

Neuroprosthetics can also be used to predict subsequent movement and to stimulate the appropriate site in the spinal cord.[8,21,22] This approach has been used clinically in a patient who had a spinal cord injury.[8] Previously recorded neural signals were decoded, then electrical stimulation was sent spatiotemporally. However, to ensure that the stimulus coincided with the patient's intention, the 3D kinematics were continuously analyzed using 14 fixed cameras, and the signaling requires decoding of electromyography (EMG) signals and neural signals in advance.[8] These neuroprosthetic systems require various additional processing devices for decoding and encoding of neural signals; these processes limit data-processing speed and consume a large amount of energy, and the devices have limited possibility of miniaturization.[8,21–24]

Neuroelectronics composed of organic materials have attractive material properties, good solution processability, and ease of molecular tuning. Organic materials can provide mechanical softness that is similar to the texture of neural tissues, has good stretchability and superior capacitance, and is biocompatible with reduced tendency to stimulate an immune response.[25–27] These characteristics are superior to those of conventional neuroelectronics, which use metal electrodes and CMOS processors and therefore have poor biocompatibility and high energy cost. Neural interfaces that are composed of organic materials and that can accurately read or stimulate various neural signals have been developed and have improved biocompatibility compared to conventional metallic neural interfaces.

Organic nervetronics is a kind of neuroprosthetics in which electrophysiological signals are relayed by the artificial synapses and neurons that mimic biological counterparts in biomimetic way instead of damaged nerves.[28,29] These devices may provide a core element for next-generation neuroprosthetics. A human body includes $\approx 10^{12}$ neurons and $\approx 10^{15}$ synapses. The neurons communicate by propagating spatiotemporal information through synapses by sending action potentials, which are voltage spikes that convey physiological signals. A synapse has the trait of plasticity, which is an adjustment of synaptic weight or transmission efficacy in response to experience.[30] By mimicking biological processing that uses voltage spikes, and by emulating synaptic plasticity, organic nervetronics enables efficient data processing in simple devices, rather than the complex data processing procedure that is necessary in conventional systems, which use CMOS technology.[31,32] Therefore, organic nervetronics is appropriate for use in future neuroprosthetics that require high efficacy, closed-loop operation, portability, and stability upon long-term implantation.

Here, we review recent progress of organic neuroelectronics, specifically neural interfacing devices that use soft electrodes and nervetronics that use artificial synapses and neurons (**Figure 1**). We introduce the material requirements of neural interface, such as electrical properties, chemical stability, mechanical properties, and biocompatibility. We present recent
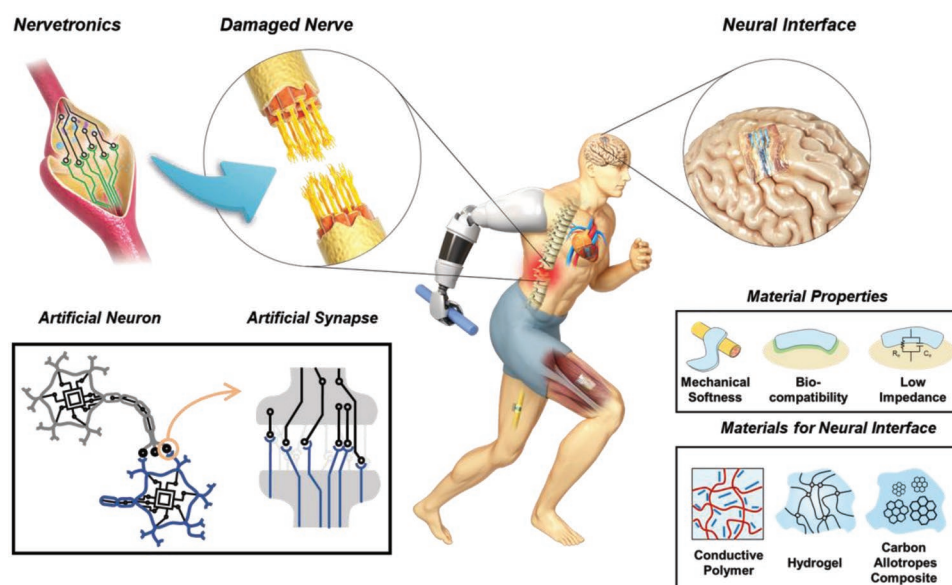

Figure 1. Schematics of organic neuroelectronics and its components.

**ADVANCED
SCIENCE NEWS**

www.advancedsciencenews.com

**ADVANCED
MATERIALS**

www.advmat.de

studies on organic materials and carbon allotropes which are promising fillers for organic composites, for use in neural interfaces to meet these requirements, then introduce examples of neural interfacing devices that use organic materials, including various device types, including neural interfaces for brain, heart, muscle signals, and optogenetics. We also present recent research on nervetronics that use organic artificial synapses for next-generation neuroprosthetics, and address the challenges that must be overcome before neuroprosthetics are suitable for clinical applications. Last, we suggest the future challenges and outlooks for development of organic neuroelectronics.

2. Materials for Neural Interfaces

For neuroelectronic systems, neurological signals can be recorded and triggered by electronic devices. For this purpose, electronic devices should operate reliably in vivo. Especially, neural interfaces interface directly with neural tissues and nerve cells, so materials for neural interfaces should be biocompatible; that is, must not be toxic or induce immune response, must be mechanically soft, chemically robust in vivo, electrochemically stable, and capable of conformal contact with cells.[33–35] Also, the materials with ionic-electric mixed conduction can equip high capacitance by being compatible with electrolyte environment and ion conduction mechanism of neural transmission by biological neurons. Some organic materials and composites of organic materials and carbon allotropes meet all of these requirements. In this section, we introduce the material requirements for neural interfaces, and review recent progress in development of organic materials (conducting polymers and hydrogel materials) and carbon allotropes, which are widely studied together with organic materials (e.g., blends, compounds, and multi-layer coatings) for neural interfaces.

2.1. Material Requirements for Neural Interface

Neural interfaces record bioelectric signals from nerve cells, and stimulate neural cells and tissues for medical diagnosis and treatment purposes. To collect neural signals or stimulate cells at high resolution and high accuracy, invasive or implantable bioelectronics systems are necessary. In this system, electrode design depends on anatomical location and on target therapeutic application.[36,37] Insertion of probe electrode and multielectrode array have been widely used due to their high spatial resolution and effectiveness to detect or stimulate signals in the deep brain region for neurological disorders such as epilepsy, and Parkinson's disease.[38–41] To be compatible with long-term implantation, the materials that compose a neural interface must not degrade, delaminate, or induce a foreign-body response after implantation.[42,43] They will be included in a high-density multielectrode array to record signals with high spatial resolution, so to ensure high accuracy and high signal-to-noise ratio (SNR), they must also have low impedance and high charge capacity. They must also be biocompatible, chemically stable, not susceptible to biofouling, and have mechanical softness that matches those of biological tissues.

2.1.1. Electrical Properties

The basic function of a neural electrode is to transmit electrical charges between neural tissues and signal processing devices. For this purpose, electrodes have been composed of materials that have high electrical conductivity. Furthermore, charge is transferred at the interface between neural tissues and electrodes. The charge transfer can be divided into non-Faradaïc (capacitive) and Faradaïc modes. In non-Faradaïc mode, electrode materials are electrochemically stable, and an electrical double layer (EDL) forms a place for capacitive charging/discharging. In Faradaïc mode, electrochemical redox reactions occur between electrode and electrolyte for charge transfer that leads to a Faradaïc reaction. By these charge-transfer processes, electrical potential of neural signals can be transferred to the electrode (recording) and electrical signals from a neural interface can be transferred to neural tissues (stimulation).[44,45]

Recording of neural signals in biological tissues is generally performed with the electrode being a short distance from the neural tissue. Electric potential such as extracellular potential or local field potential (LFP) is generated by the action potential of a neuron. This potential can be easily disturbed by noise (both biological and device noise), so the arrangement must have high SNR to ensure that the recording electrode can distinguish signal from background noise. Assuming that an electrode is a perfect point, the recorded electric potential V_{rec} can be described as (**Figure 2**a, left)

$$V_{rec} = \frac{I_{AP}}{4\pi\sigma r}\left(\frac{1}{R_e} + j\omega C_e\right)R_{ic} \qquad (1)$$

where I_{AP} is the transmembrane current during action potential firing, σ is the conductivity of extracellular electrolyte, r is the distance from the electrode, R_e is the leakage resistance, j is the imaginary unit, ω is the angular frequency of the action potentials, C_e is the capacitance of the electrode by capacitive charge injection, and R_{ic} is the interconnect resistance.[36,47,48] To achieve high SNR, V_{rec} must be larger than the noise level.[36,47,48] Therefore, C_e and R_{ic} must be high and R_e must be low.

Stimulation of neural tissues by a neural interface induces transmission of electric signals to neurons. Charge transfer between electrode and electrolyte enables transmission of the electric signal. During stimulation, charges are injected from electrode to electrolyte, then an electrical potential is generated on targeted tissues and neurons. Therefore, to stimulate the electrode, the generation of electrical potential on neural tissue must be accurate and efficient. Stimulation electrodes generally use non-Faradaïc mode, because high-voltage stimulation can induce undesired reactions in Faradaïc mode.[49] Electrical potential V_e of neural tissue can be calculated by considering an equivalent circuit (Figure 2a, right)

$$V_e = \frac{V_{sti}}{4\pi\sigma r}\left(\left(\frac{1}{R_e} + j\omega C_e\right)^{-1} + R_{ic}\right)^{-1} \qquad (2)$$

where V_{sti} is stimulation voltage, and other variables are as in the previous equation.[47,48] According to the equation, effective stimulation requires high C_e, low R_{ic}, and low R_e.[50,51]
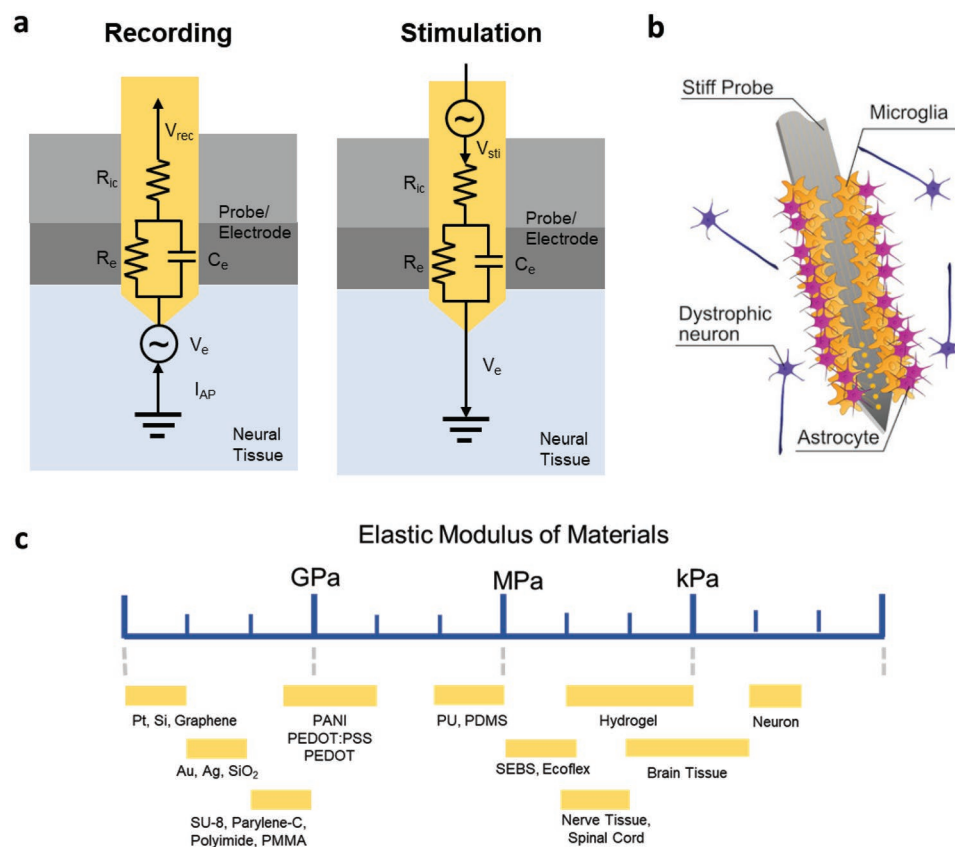
Figure 2. Requirements for neural interfaces. a) Equivalent circuit diagrams of electrode/neural tissue interface in the case of recording (left), and stimulation (right). b) Immune response to probe electrode. c) Elastic modulus of various materials for neural interface and biological tissues. b) Reproduced under the terms of the CC-BY Creative Commons Attribution 4.0 International license (https://creativecommons.org/licenses/by/4.0).[46] Copyright 2021, The Authors, published by Wiley-VCH.

During the charge-transfer process, charge-injection capacity (CIC), charge-storage capacity (CSC), and impedance are generally evaluated to determine the efficiency of the electrode. CIC represents stimulation efficacy of electrode, that is, the amount of injected charge across the electrode–electrolyte interface per unit surface area during the leading stimulation pulse.[49,52] CSC is the amount of charge per unit surface area, that can be stored in the electrode.[49] CIC and CSC are closely related to C_e of the electrode, so high charge-transfer efficiency requires high CSC and CIC.[53,54] Also, the impedance of electrodes is determined by R_e and C_e, so low impedance is also desired. However, undesired Faradaïc reactions can occur, such as redox reaction of water, corrosion of metal, or evolution of gas.[33] These undesired reactions can reduce charge transfer or even damage the neural tissues.[55] To mainly induce electrolyte–electrode charge transfer, the charge-transfer capacity has a maximum limitation. Also, irreversible electrochemical redox reaction can induce metal/electrolyte interface vulnerabilities including low signal accuracy caused by current fluctuations, and noise signals caused by denaturation of electrodes or electrolytes. The denaturation can be caused by redox reactions of electrode materials such as reactive metals and organic materials.[56,57] For example, a polypyrrole (PPy) backbone can be oxidized irreversibly by nucleophilic attack on pyrrole rings by OH⁻.[57] These undesired and irreversible Faradaïc reactions

lead to poor electrochemical stability of neural electrodes upon repetition of charge injection/storage cycles. Therefore, design of electrode materials must also consider electrochemical stability and this limitation.

However, high parasitic capacitance causes current leakage to adjacent tissues. It is unavoidable if an insulation coating layer is not used. Insulating layers generally have high dielectric constant to block charge conduction from other tissues or electrodes. The equivalent circuit of single neural electrode can be described as a low-pass RC filter with cut-off frequency f_c and attenuated voltage V_{out} that leaks out of electrode into untargeted tissues:

$$f_c = \frac{1}{\omega RC}, \; V_{out} = \frac{1}{\sqrt{1 + \omega^2 R^2 C^2}} \tag{3}$$

where ω is the angular frequency of the signal waveform, R is the resistance of the insulating layer, and C is its capacitance.[33] Therefore, to reduce voltage attenuation, the material used in the insulating layer must have high C. However, to reduce cross-talk between adjacent electrodes, the insulating layer must have both low C and high R.[58] Therefore, insulating materials that have low dielectric constant such as parylene and silicon oxide with appropriate thickness design are widely used for the insulating layer. Considering the

**ADVANCED
SCIENCE NEWS**

www.advancedsciencenews.com

**ADVANCED
MATERIALS**

www.advmat.de

aforementioned properties, electrode and dielectric materials can be developed to design reliable efficiency of the stimulating neural electrode.

2.1.2. Chemical Stability

Implantable neural interfaces require materials that are stable for a long time. Biological neurons are bathed in an electrolyte, and in this environment, metals in the conductive layer (e.g., Au and Ir) and adhesion layer (e.g., Ti) of the implant can form a galvanic cell; thus, corrosion occurs.[59] Electrodeposition of conductive polymers (CPs) onto electrode is an effective way to reduce corrosion.[60,61] CPs such as poly(3,4-ethyelne dioxythiophene) (PEDOT) and PPy are chemically stable and highly conductive in water. Furthermore, oxidation of the polymer precedes corrosion of the metal electrode, so the CP can polymerize and coat the metal electrode to protect it. However, the anticorrosion CP can delaminate from the electrode. The adhesion of CP coating can be increased by using additives and self-assembled monolayers (e.g., organosilane moiety) to cross-link adhesion.[62–65]

Materials for neural interfaces must also promote or facilitate neuronal growth or adhesion. For this purpose, organic materials have the advantage of that their surface properties can be easily tuned by substituting their functional groups. Especially, a positively charged group can promote adhesion of the cell membrane, which is negatively charged. Thus, materials that bear positively charged groups, such as polyelectrolyte with aminosilane groups, are widely used as coating materials to strengthen cell adhesion.[66] However, biofouling, which is undesired non-specific adsorption of proteins, must be reduced; it occurs due to contact with biological fluids in vivo. Biofouling can be reduced by surface functionalization to increase hydrophilicity (e.g., functionalization with polyethylene glycol or poly(ethylene glycol) methacrylate (PEGMA)) or by incorporation of anti-biofouling materials.[67]

2.1.3. Biocompatibility

When an electrode is inserted into a neural tissue, it may mount a foreign body response to resist the invasion. The response can be acute or chronic. The introduction of electrodes disrupts glial cells, which structurally support neurons and conduct synaptic signals. The disrupted communication of glia induces release of cytokines and increase in the number of activated microglia and reactive astrocytes (Figure 2b).[42,46] Also, inflammatory responses (such as macrophages, monocytes, and neutrophils) are induced. Especially, macrophages lead to formation of fibrin deposits on the electrode, with consequent tissue encapsulation.[43] This encapsulation blocks charge transfer and transmission of neurotransmitters, so adjacent tissue cannot react as normal brain tissue does.[68] Therefore, to ensure that the neural interface can communicate effectively with neural tissues, the foreign-body response must be minimized.

To reduce foreign-body response, the physical properties of the electrode are important. First, reduction of device size

can decrease the risk of damage to the tissue. Use of small devices can reduce the volume of the damaged cell region and the consequent inflammatory response and scarring.[53] However, reduction of device size can also reduce its CSC.[69] Thus, the device size should be chosen to balance the biological and electrical properties. Second, use of soft materials for neural electrode can reduce damage caused by chronic micromotions of tissues during life activity. Neural cells and tissues typically have an elastic modulus <10 kPa. However, conventional metal electrodes have elastic modulus >1 GPa, so they have a large mechanical mismatch with tissues; to reduce it, various flexible and stretchable electrodes have been developed using soft organic and carbon materials (Figure 2c).

However, the penetration electrode must have appropriate stiffness to permit insertion into neural tissues. When soft electrode materials are used, buckling failure can occur; when this happens, the neural electrode cannot be properly inserted. The buckling force F_B can be described as

$$F_B = \frac{\pi^2 I E}{k_e^2 L^2} \tag{4}$$

where I is the moment of inertia, E is elastic modulus of materials, k_e is the effective length factor, and L is the electrode length.[70] To increase F_B, E must be high, but to reduce mechanical mismatch between neural interfaces and neuronal tissues, E should be low. Therefore, several strategies have been suggested to support insertion of soft electrodes that have low elastic modulus.[15,71–73] For example, the soft neural interface is placed on a rigid SU-8 shuttle during insertion, and then the soft electrode on a parylene film is delaminated from the SU-8 shuttle, which is then physically removed. Because of weak adhesion between parylene film and SU-8 shuttle, water absorption from cerebrospinal fluid delaminates soft electrode from the SU-8 shuttle without loss of electrical characteristic.[74]

Cytotoxicity and biocompatibility must also be considered. For example, dissolution of metal ions can cause toxicity that is inappropriate for long-term insertion.[56] To fabricate an electrode that has long-term stability, biocompatible materials such as proteins have been developed for use as a coating layer or an adhesion layer.[75] These materials reduced the inflammatory response and maintained high cell viability in vitro.

2.2. Emerging Organic Materials for Neural Interfaces

The traditional materials for neural interface are metal and silicon materials, but they have been too rigid and have low capacitance. To overcome these limitations, organic materials have been developed to meet a wide range of material requirements (electrical properties, chemical stability, and biocompatibility) for use in neural interfaces. In this section, we consider CPs, carbon allotropes which can be used as conductive fillers for the organic composites, and hydrogel composites.

2.2.1. Conductive Polymer

CPs have been widely evaluated as neural-interface materials because of their ionic and electrical conductivity, and their

tunable mechanical, electrical, and chemical properties. The first discovered CP was polyacetylene, which has electrical conductivity that is comparable with those of metals. The electrical conductivity of CPs originates from π-orbital overlap that is provided by alternating repetition of single and double bonds in the conjugated polymer backbone.[76] This high electrical conductivity is suitable for applications in neural electrodes.

Ion-permeable CPs have porous and rough morphology that allows ion migration and penetration toward bulk polymer. Ion penetration into CPs enables high volumetric capacitance by molecule-level formation of an EDL and rapid Faradaïc reaction between bulk CPs and penetrated ions.[47,77,78] This trend causes large decrease in electrochemical impedance and increase in capacitance of the neural electrode; the capacitance increase improves CSC and CIC, and increases the SNR.[27]

Various kinds of CPs have been evaluated as coating material for neural electrodes. Polyaniline (PANI) has high electrical conductivity (100–200 S cm^{-1}) in its emeraldine electrochemical state (half oxidized). However, PANI has poor cell adhesion, poor biocompatibility, and poor processability, and its electrical conductivity decreases at the pH of human body (pH ≈ 7.4).[79] PPy is widely used and has high electrical conductivity, biocompatibility, and chemical stability. The monomer has high solubility in water, and is therefore compatible with solution processing.[80] PEDOT has high electrical conductivity with superior chemical stability and in vivo biocompatibility.

These CPs are easily synthesized or coated by various methods including chemical polymerization, electrochemical polymerization, spin-coating, dip-coating, and chemical vapor deposition. Electrochemical polymerization is generally preferred for implanted neural electrodes due to the stability of CPs in the biological environment.[27,79] Especially, electrochemical polymerization of PPy and PEDOT is widely used to coat neural electrodes, because this process provides electrodes with excellent electrical properties. For example, a parylene-C neural probe coated with PEDOT (by electrochemical polymerization) shows higher SNR than an Au electrode (**Figure 3**a).[81] The PEDOT coating also increases electrode capacitance due to nanostructured morphology that reduces noise. The electric hum of a PEDOT-coated electrode at 50 Hz is a tenth that of an electrode without a PEDOT layer. Also, cell viability after 168 h is 40 times higher when the electrode is coated with PEDOT than when it is not.

Negatively charged dopant ions neutralize the unstable oxidized backbone. Therefore, chemical stability of CP is further increased after dopant addition. Dopant introduced in CPs can improve electrical conductivity by forming ionic complexes such as polarons, bipolarons, or solitons. Various dopants are studied in CP such as the large polymeric dopant poly(styrene sulfonate) (PSS), and the small dopant paratoluene sulfonate (pTS).[83,84]

The properties of CPs are dependent on dopant types (Figure 3b). When various types of dopant are added to PEDOT film, the smoothest surface morphology was obtained using PEDOT doped with PSS; that is, the largest dopant.[84] PEDOT films doped with small molecules such as ClO_4, pTS, or benzenesulfonate develop rougher morphology than PSS-doped PEDOT. The surface morphology of a film affects its electrochemical property. CPs doped with small molecules and that form rough films have large surface area, which imparts high CSC. For example, initial CSC is 150.5 mC cm^{-2} for ClO_4-doped PEDOT has but only 100.0 mC cm^{-2} for PSS-doped PEDOT. However, the roughness of CP surface and the cytotoxicity of dopants also affect the neural outgrowth and attachment for
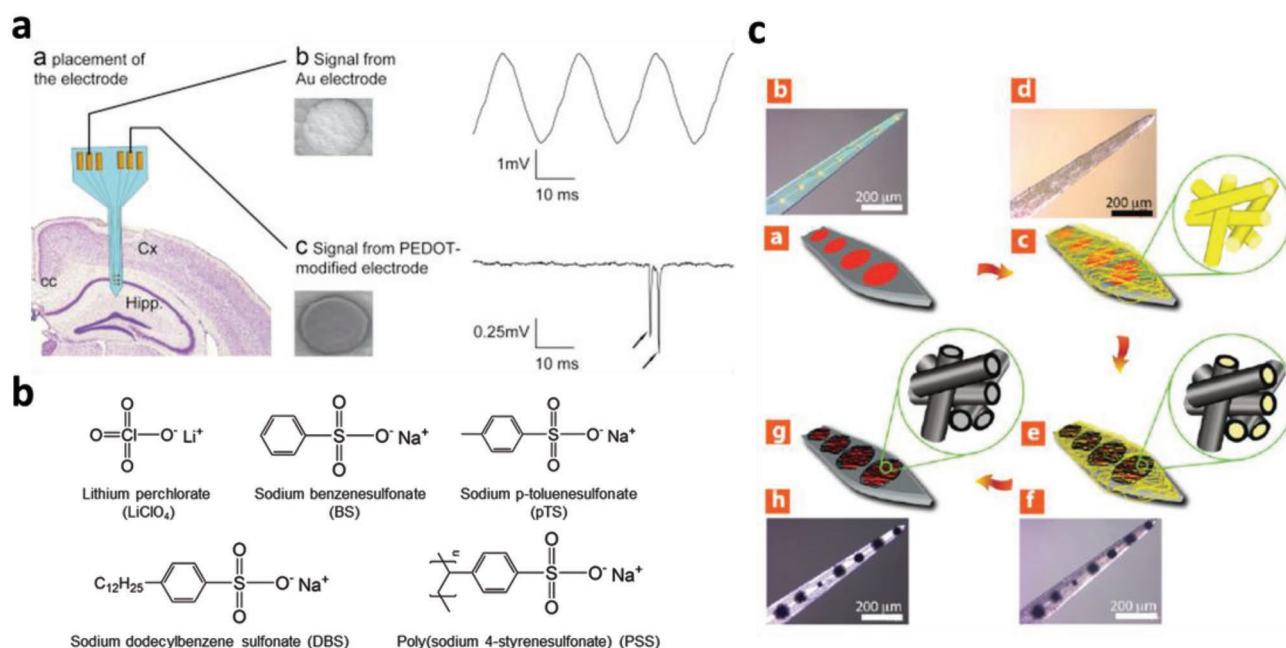

Figure 3. Conductive polymers for neural interface. a) Improved SNR of electrochemically polymerized PEDOT-coated electrode compared with Au electrode. Reproduced with permission.[81] Copyright 2015, Elsevier. b) Chemical structures of various dopants for conductive polymer. c) Schematic illustrations and optical images of conductive polymer nanotube. PPy and PEDOT nanotubes are electrochemically deposited on electrospun PLLA fibers, which are removed in the final stage. c) Reproduced with permission.[82] Copyright 2010, Wiley-VCH.

neural electrode.[84] Therefore, dopant can be selected to engineer mechanical and electrochemical properties.

CP nanotubes (NTs) have also been evaluated for their ability to modify the surfaces and electrochemical properties of CP films.[82,85] In a commercial Michigan neural electrode, poly(L-lactic acid) (PLLA) nanofibers are electrospun to form an NT, and then PPy and PEDOT are electrochemically deposited. Then the PLLA templates are removed by dissolving them with dichloromethane (Figure 3c).[82] The resulted NT composed of PPy and PEDOT has very large surface area, and therefore low electrical impedance (19.5 kΩ for PPy and 2.5 kΩ for PEDOT at 1 kHz) and high charge capacity density (184 mC cm^{-2} for PPy and 392 mC cm^{-2} for PEDOT). Also, the adhesion between cells and CP NTs is improved, so culture cells remain more intact than when the NTs are not formed.

2.2.2. Carbon Allotropes

Conjugated carbon allotropes have been studied as conductive nanomaterials that are coated, composited, or blended with organic materials.[47,86–88] The conjugated carbon allotropes have high electrical conductivity and large surface area due to their low-dimensional structure which provides high CIC and SNR for neural electrodes.[87,89] Also, the carbon allotropes can have mechanical flexibility, biocompatibility, and chemical stability in a biological environment.[53,86,89] Research has mainly focused on carbon fiber, graphene, and carbon nanotubes (CNTs).

Carbon Fiber: Carbon fiber is mainly used for small-diameter (4–10 µm) microelectrodes that record extracellular and intracellular neural signals. The small dimension of a carbon-fiber electrode results in minimal invasive cross section and thereby induces negligible immune response, and also provides high spatial resolution.[53] However, carbon fiber is relatively stiff, so it does not match the pliability of biological tissues.[90] Also, the carbon fibers are insulated with fused-silica or glass fibers that increase the size of the electrodes. These disadvantages limit the use of the carbon fiber as implantable in vivo neural electrodes. To solve these limitations by reducing the size of the insulation (e.g., fused silica capillary), an insulating coating layer of carbon fiber has been demonstrated.[91]

Other coating materials to improve electrochemical property of carbon fibers have also been evaluated; examples include CP such as PEDOT:PSS, iridium oxide, and carbon nanowalls.[67,92,93] These coating materials can be applied sequentially on carbon fibers. In one example, parylene-N was coated by CVD onto carbon fiber as an insulator that has a frequency-invariant property, then itself coated with functionalized polymer, poly((p-xylylene-4-methyl-2-bromoisobutyrate)-*co*-(p-xylylene)) by CVD polymerization (**Figure 4**a); then the polymer was coated with a PEGMA layer by atom-transfer polymerization to provide protein resistance and thereby improve biocompatibility.[67] This serially coated microthread electrode had flexibility compliance of 220 µm N^{-1} in the axial direction whereas an Si probe had 4.04 µm N^{-1}. Thus, biofouling and bleeding are extremely decreased due to the mechanical property which is compliant with brain tissue. The foreign-body response was also reduced. Also, a PEDOT:PSS-coated

neural probe fabricated by electrochemical polymerization has improved electrochemical properties, and therefore an increased SNR (bare carbon fiber: 4.71; coated carbon fiber: 12.7) in vivo.

Graphene: Graphene is a 2D hexagonal array of sp^2-bonded carbon, and has a large effective surface area. Graphene has many attractive properties for use in neural interfaces: mechanical flexibility, non-toxic property, optical and magnetic transparency (i.e., compatibility with magnetic resonance imaging [MRI]), and strong resistance to corrosion or oxidation.[86] Especially, graphene has high neuronal affinity that improves cell growth.[97] Graphene is a sheet, so graphene and graphene-derived materials have been coated on neural electrodes. A monolayer graphene sheet can be fabricated by CVD on copper foil, and then transferred to another substrate. A graphene layer was deposited on a copper (Cu) microwire neural electrode. Cu is toxic, so a Cu electrode is inappropriate for use as neural electrode. The encapsulation by graphene significantly increased cell viability after 48 h (≈5% without graphene, >93% with graphene) (Figure 4b).[94] The graphene-encapsulated Cu microwire neural electrode was compatible with MRI. Graphene can be transferred to metal or metal oxide. The biocompatibility of a commercial Michigan-type neural probe can be improved by coating it with graphene. When graphene is transferred onto IrO$_x$, detection efficiency of intracortical signal was 50%, whereas it was 10% by an uncoated electrode (Figure 4c).[95]

Carbon Nanotubes: CNTs are rolled-up graphite sheets that be composed of single (single-walled CNT) or multiple-walled sheets (multiwalled CNT: MWCNT). CNTs have also been evaluated for use as neural interfacing materials due to their large surface area (700–1000 m^2 g^{-1}), high aspect ratio, high mechanical strength, great electrical properties such as high conductivity, and biocompatibility.[98] Therefore, CNT-coated neural electrodes or CNT microfiber neural electrodes can provide high charge-injection capacitance, low impedance, and biostable property. For example, MWCNTs were coated on indium-tin oxide (ITO) neural electrode by electrochemical deposition using MWCNTs suspended in potassium–gold cyanide aqueous solution.[89] CNT coating decreased the impedance of ITO electrode from 748 to 32 kΩ, and increased charge transfer (indicated by parallel capacitance) by 45 times (Figure 4d).

The CNT fiber electrode can be fabricated using a spinning method. For instance, CNT solution with chlorosulfonic acid can be extruded into coagulant through a spinneret.[99] Formed filaments are collected on a rotating drum to form highly aligned CNT fibers. For neural fiber electrodes, CNTs must be insulated by a polymer such as polystyrene–poly(1,4-butadiene), (PS-b-PBD), so that only the tip is exposed to contact the neural tissues. A CNT fiber electrode coated with PS-b-PBD has superior electrical and electrochemical properties compared to the conventional metal electrode.[96] CNT fibers have large electrochemically active area, so a CNT-fiber electrode has low impedance and high CSC. Compared to a PtIr wire of the same diameter, a CNT fiber has 1/15 the impedance and 450 times the CSC (Figure 4e). Also, CNT fiber electrode shows stable recording and low inflammatory response upon long-term implantation.
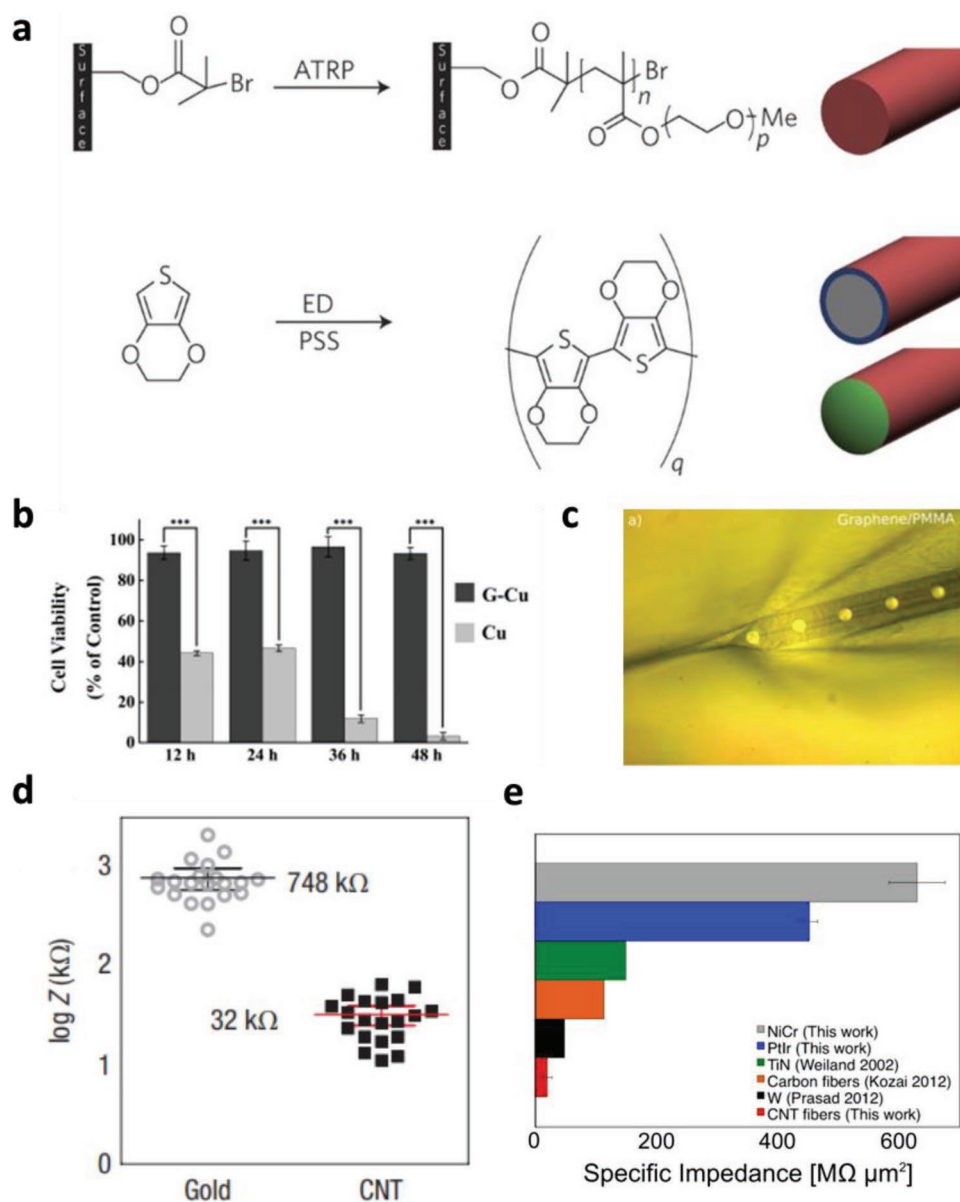
**ADVANCED
SCIENCE NEWS**

www.advancedsciencenews.com

**ADVANCED
MATERIALS**

www.advmat.de

Figure 4. Carbon allotropes for neural interfaces. a) Schematic illustrations to fabricate microelectrode using on carbon fiber. Poly(ethylene glycol) methacrylate was deposited on functionalized poly(p-xylylene)-coated carbon fiber for protein resistance, and PEDOT:PSS was electrochemically deposited for active electrode area. Reproduced with permission.[67] Copyright 2012, Springer Nature. b) Normalized PC-12 Cell viability of graphene-encapsulated copper microwire (G–Cu) and copper wire for various times. Reproduced with permission.[94] Copyright 2012, American Chemical Society. c) Optical images of graphene-transferred Michigan type probe. Reproduced with permission.[95] Copyright 2019, Wiley-VCH. d) Impedance of CNT-coated multielectrode array and gold-coated multielectrode array. Reproduced with permission.[89] Copyright 2008, Springer Nature. e) Specific impedance at 1 kHz of CNT fiber microelectrode and various electrode materials. Reproduced with permission.[96] Copyright 2015, American Chemical Society.

2.2.3. Hydrogel Composites

Hydrogels are cross-linked hydrophilic polymer networks. They have been widely evaluated for use as neural interfacing materials. The elastic modulus (1–100 kPa) of hydrogel is the most similar to biological tissue among the previously reported neural interfacing materials. This similarity between neural tissues and electrode minimizes mechanical mismatch that can cause tissue damage and induce a foreign-body response.[100] Hydrogels are water-permeable and ionically permeable; thus,

electrolyte can penetrate into bulk hydrogel. Therefore, the capacitance of the electrode is proportional to its volume; this phenomenon is known as volumetric capacitance. It is much larger than areal capacitance, which occurs in impermeable electrodes, so hydrogel has better charge-transport characteristics than metal or metal oxide electrodes.[47] Because of these attractive characteristics, hydrogel has been developed for future neural interfacing materials.

In addition to mechanical softness and volumetric capacitance that originated from ionic conductivity, high electrical

conductivity of hydrogel is also required for neural interface. However, most hydrogel materials (e.g., poly(acrylamide) (PAAm), poly(vinyl alcohol), poly(acrylic acid) (PAA), and poly(ethylene glycol)) have low electrical conductivity, so several strategies have been evaluated to increase it. They can be divided into two categories: 1) addition of electrically conductive components to template hydrogel materials that have an insulating property, and 2) developing conducting polymer hydrogel by cross-linking with a CP.

Various electrically conductive materials can be added into hydrogel materials including CPs, carbon allotropes, and metal nanomaterials. The CPs include PEDOT:PSS, PANI, and PPy, which are mixed with template hydrogel precursors (e.g., PAAm and PAA).[101–103] For example, PEDOT:PSS, cross-linker, and thermal initiator can be mixed with acrylamide monomer.[104] The mixed solution can be coated on gold substrate and thermally cured to make soft conductive PAAm-PEDOT:PSS hydrogel (**Figure 5**a). Due to large volumetric capacitance of the hydrogel, the PAAm-PEDOT:PSS hydrogel has CSC = 13.9 mC cm^{-2}, whereas PEDOT:PSS has CSC = 11.1 mC cm^{-2}. Furthermore, the elastic modulus of the hydrogel can be tuned in the range of 10–100 kPa by adjusting the mixing ratio.

Although use of additives to hydrogels can increase their electrical properties, the strategy has the limitation that the insulating template polymer composes most of the hydrogel. To overcome this limitation, the conducting polymer itself can be a hydrogel. To achieve a conducting-polymer hydrogel, self-assembly and cross-linking approaches have been developed.[109,110] A pure PEDOT:PSS hydrogel can be obtained by mixing a large amount (up to 50 vol%) of volatile additive (dimethyl sulfoxide, DMSO) to PEDOT:PSS aqueous solution.[105] Without DMSO addition, PEDOT:PSS forms only microgel fragments after a drying and swelling process. After addition of DMSO, PEDOT:PSS aqueous solution can be recrystallized to form PEDOT-rich nanofibrils, and chains can be rearranged by dry-annealing (Figure 5b). The pure PEDOT:PSS hydrogel has attractive characteristics for use as a neural interface, including high electrical conductivity (≈20 S m^{-1} in phosphate-buffered saline), high CSC (≈60 mC cm^{-2}), and low elastic modulus (≈2 MPa). To further improve electrical conductivity, 50 wt% of ionic liquid, 4-(3-butyl-1-imidazolio)-1-butanesulfonic acid triflate, is blended into PEDOT:PSS.[106] The blended ionic liquid promotes aggregation of PEDOT and formation of interconnected polymer networks. During the washing process, ionic liquid (not biocompatible) and excess PSS (insulating species) are washed out; the resulting hydrogel has better properties than pure PEDOT:PSS hydrogel such as reasonable electrical conductivity (≈47.4 S cm^{-1}), high CSC (≈164 mC cm^{-2}), and low elastic modulus (≈32 kPa) (Figure 5c).

Conducting interpenetrating networks (c-IPNs) can be achieved by in situ polymerization to further improve the mechanical properties of PEDOT:PSS hydrogel.[107] First, loosely packed PEDOT:PSS hydrogel is formed by mixing it with ionic liquid. Then acrylic acid (monomer), chemical cross-linker, and thermal initiator are mixed and infiltrated into the hydrogel. Finally, polyacrylic acid c-IPNs are achieved by in situ polymerization of acrylic acid (Figure 5d). The process yields a very low elastic modulus of 8–374 kPa which is similar to that of

biological tissue (0.5–500 kPa) while retaining high electrical conductivity (>10 S m^{-1}) due to the connectivity of the PEDOT:PSS.

Carbon allotropes can also be added into hydrogel templates to increase the conductivity of the hydrogel, due to their high electrical conductivity and reliable chemical stability in vivo.[111] Carbon allotropes are easily functionalized chemically, and can be added to various kinds of biocompatible hydrogels such as poly(ethylene glycol), poly(vinyl alcohol), collagen, gelatin, and chitosan.[47] By addition of CNT, electrical percolation networks can be formed in hydrogel templates. These CNT-hydrogel nanocomposites have excellent mechanical and electrical properties for use in neural interfaces. Hydrogel-CNT composites that use supramolecular β-peptide have high electrical conductivity.[88] The β-peptide, which self-assembles, was chosen as a molecular component to construct a hierarchical complex with CNTs as axially assembled nanofibers to increase biocompatibility of CNT (Figure 5e).

Graphene derivatives have also been used in hydrogel to improve conductivity and adhesion. Graphene oxide (GO) is a functionalized 2D nanosheet that has high biocompatibility and large surface area. The GO can be a template for self-assembly in hydrogel. For example, GO can be modified with sulfonated and catechol groups to form PDA-grafted graphene oxide (PSGO).[108] PEDOT can be assembled on PSGO to form PSGO-templated PEDOT (PSGO-PEDOT) by interaction between PEDOT and PSGO. The PSGO-PEDOT has high conductivity of 829 S m^{-1} because the sulfonated group acts as a dopant for PEDOT. Also, catechol groups are redox-active and this trait provides good surface adhesion. When PSGO-PEDOT nanosheets are incorporated into a PAAm hydrogel network (Figure 5f), the resulting complex hydrogel shows high electrical conductivity (108 S m^{-1}), increased maximum tensile strength (2000%), and high fracture energy (3750 J m^{-1}).

3. Organic Neural Interfaces

Metal electrodes collected into MEAs can probe and stimulate activity of multiple neurons at high spatiotemporal resolution. Results obtained using MEAs have significantly contributed to the understanding and development of neuroscience over the past decades.[9,112] Nevertheless, metal microelectrodes that use electron conduction to transmit electrical signals, and that interface with nerve cells that use ionic conduction to transmit bioelectric signals, have the relatively low charge-capacitance of noble metals (Au, Pt, and Ir, which have an areal capacitance) compared to organic materials (which have a volumetric capacitance and this low volumetric capacitance significantly decreases the interfacial impedance).[25,47,113,114] In addition, rigid metal electrodes do not form conformal contact with soft cells, and therefore degrade the signal recording quality.[115] Also, MEAs can induce an immune response that results in deposition of insulating glial scar tissue, can undergo electrochemical reactions that degrade the long-term stability, and can damage cells due to the injection of a large current to overcome the low CIC.[25,116]

In contrast, organic materials have a similar molecular structure to biological cells, and therefore form conformal contact with them, and provide high charge capacity and low impedance.[17,117] Therefore, organic materials are being evaluated as interface
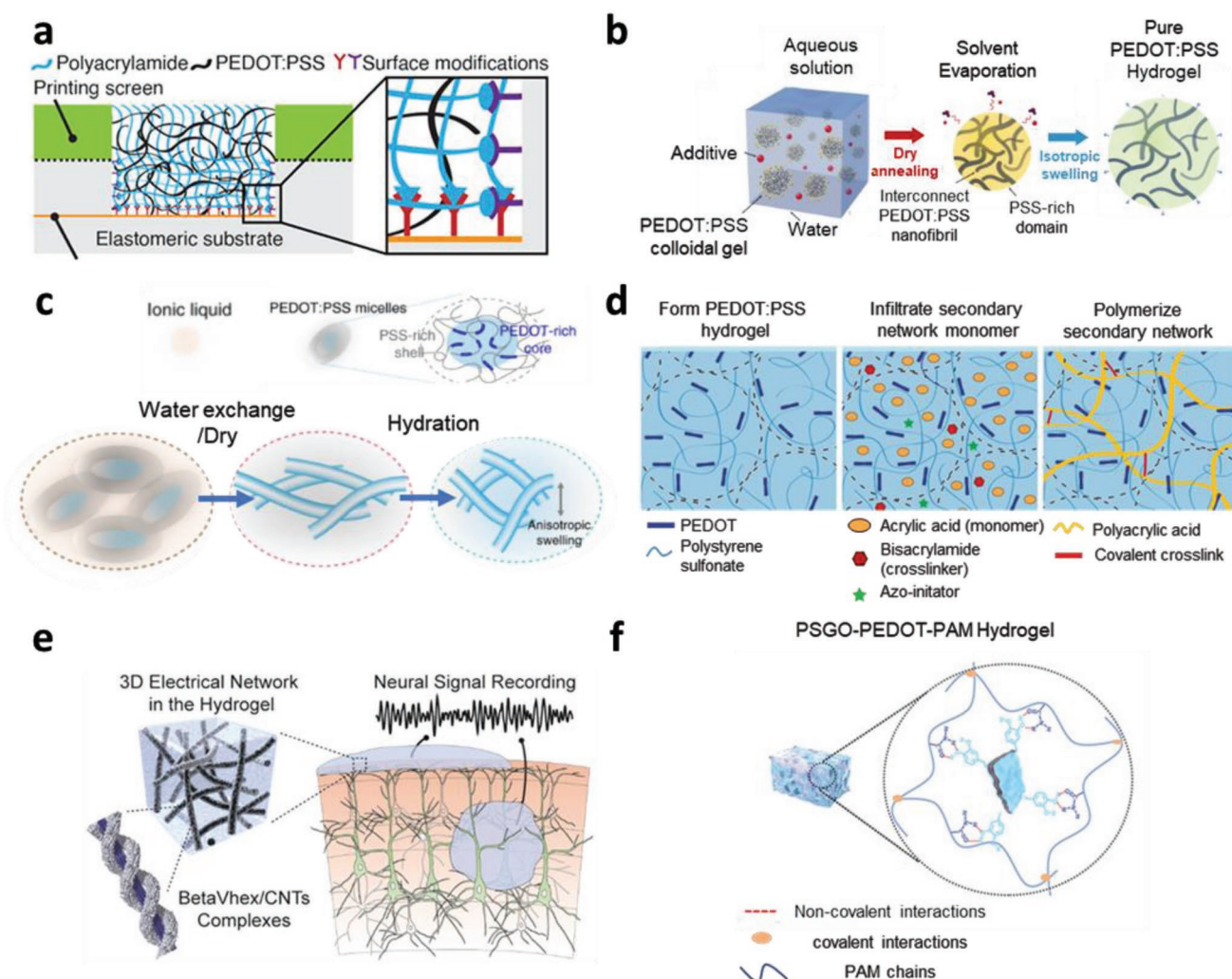
ADVANCED
SCIENCE NEWS
www.advancedsciencenews.com

ADVANCED
MATERIALS
www.advmat.de

Figure 5. Hydrogel materials for neural interfaces. a) Schematic diagrams of conductive PAAm-PEDOT:PSS hydrogel coating. Reproduced with permission.[104] Copyright 2020, American Chemical Society. b) Schematic illustrations of pure PEDOT:PSS hydrogel fabrication. Addition of DMSO stimulates interconnection of PEDOT:PSS. Pure PEDOT:PSS hydrogel formed after dry-annealing and swelling process. Reproduced under the terms of the CC-BY Creative Commons Attribution 4.0 International license (https://creativecommons.org/licenses/by/4.0).[105] Copyright 2019, The Authors, published by Springer Nature. c) Schematic of preparation of highly conductive PEDOT:PSS hydrogel. After blending of ionic liquid, water exchange, drying and hydration, excess PSS is removed and an interconnected PEDOT network is formed. Reproduced with permission.[106] Copyright 2019, The Authors, published by Springer Nature. d) Schematic illustrations of c-IPN hydrogel. (i) PEDOT:PSS hydrogels are formed by ionic liquid addition. (ii) Acrylic acid, bisacrylamide, and an azo-initiator are added into PEDOT:PSS hydrogel. (iii) Polyacrylic acid network and resulted c-IPN has formed by cross-linking of additives. d) Reproduced under the terms of the CC-BY Creative Commons Attribution 4.0 International license (https://creativecommons.org/licenses/by/4.0).[107] Copyright 2018, The Authors, published by Springer Nature. e) Schematic illustration of supramolecule peptide-CNT composite electrodes. Reproduced with permission.[88] Copyright 2020, American Chemical Society. f) Schematics of PSGO–PEDOT–PAM hydrogel. Reproduced with permission.[108] Copyright 2020, Wiley-VCH.

materials that can circumvent the limitations of metal electrodes. In the next subsection, we will review electrophysiological signal detection using organic and hydrogel electrochemical electrodes and organic electrochemical transistors (OECTs), and also review organic optoelectronic nerve-stimulation interfaces.

3.1. Neural Interface for Brain Signals

An EEG is an electrophysiological measurement that records the electrical activity of the brain. The process involves attaching a number of electrodes over a wide range on the scalp.[118,119] Although the operation and function of various parts of the brain can be checked in a non-invasive manner with high temporal resolution, the spatial resolution is low due to the long distance from the nerve cells and to the low signal transmission through the skull, so the recording measures the overall activity of a large number of synchronized nerve cells.[120] A stereoscopic electroencephalogram (sEEG) is a recording method that uses an invasive electrode that penetrates the brain.[121,122] The distance between the electrode and the spiking neuron is small, so sEEG is the most accurate method to measure the signal of a

single neuron to high spatiotemporal resolution. However, cells can be damaged by the invasive electrode.

Electrocorticography (ECoG) is widely used to monitor neural activities of the cerebral cortex at the exposed surface of the brain for clinical (e.g., for epilepsy and diagnosis of brain tumors) and research (e.g., brain-machine interface) purposes.[123,124] ECoG uses a flexible and thin electrode grid that interfaces with the brain surface in the subdural region, then records neural activities with high spatiotemporal resolution and high SNR. ECoG is minimally invasive to implant a neural interface under the skull, and less invasive than sEEG in which thin wire electrodes penetrate the blood–brain barrier and interface with tissues deep in the brain (e.g., for Parkinson's disease).

3.1.1. Organic Electrochemical Electrodes

A neurogrid has been developed, composed of a photolithographically patterned conducting polymer PEDOT:PSS/Au electrode array on 4 μm-thick parylene C film. The grid was biocompatible and ultraconformable to the brain surface (**Figure 6**a).[125,126] These traits made it appropriate for use for in vivo ECoG measurements. The PEDOT:PSS/Au electrode layer was placed at the neutral mechanical plane in the parylene C film, so mechanical stress was minimized under bending strain. The neurogrid was attached to the somatosensory cortex of a rat, and an sEEG silicon probe was also inserted into the cortex near the neurogrid to compare the recorded neural signals (Figure 6b). The signal accuracy was higher for the
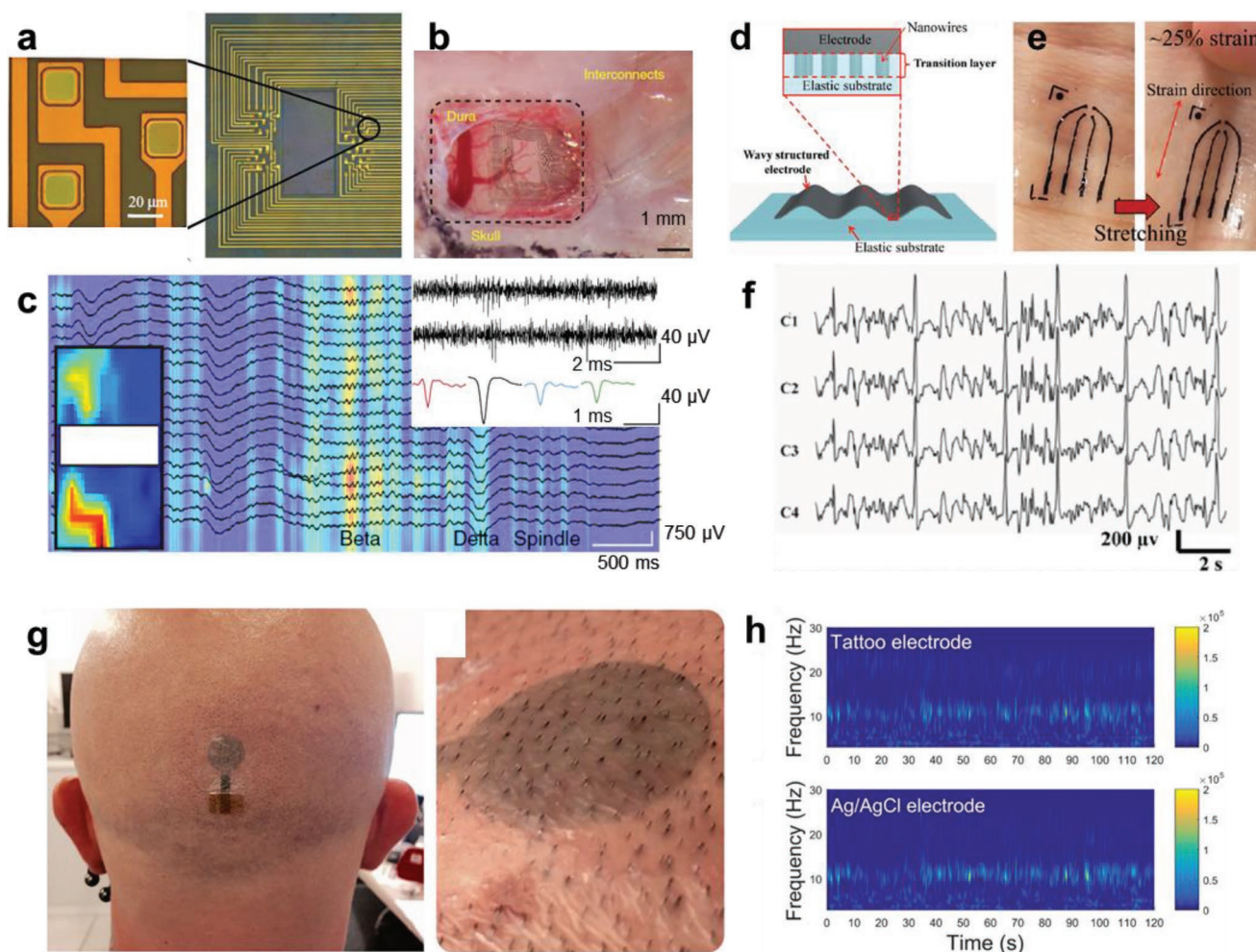

Figure 6. Neural interfaces composed of organic electrochemical electrodes for brain-signal recording. a) Microscopy images of a photolithographic-patterned conducting polymer PEDOT:PSS/Au electrode array on 4 μm-thick parylene C film. A silicon probe was inserted through the hole in the middle area. b) Digital image of the NeuroGrid on the surface of the rat somatosensory cortex. c) Time-frequency spectrogram and multichannel LFP recording of NeuroGrid during intraoperative anesthesia (inset: recordings of spiking activity). a) Reproduced with permission.[125] Copyright 2011, Wiley-VCH. b,c) Reproduced with permission.[126] Copyright 2014, Springer Nature. d) Schematic of stretchable neural interface that uses PPy NW, with high stretchability and strong substrate adhesion. e) Digital image of the stretchable neural interface that uses PPy NW, on the wrist before and after 25% stretching. f) Recorded ECoG signals from four-channel-PPy NW stretchable neural interface on the rat brain. d–f) Reproduced with permission.[127] Copyright 2017, Wiley-VCH. g) Digital images of conducting polymer tattoo electrode attached to a scalp. h) Time-frequency spectrogram of alpha wave recordings with tattoo and conventional Ag/AgCl electrodes. g,h) Reproduced under the terms of the CC-BY Creative Commons Attribution 4.0 International license (https://creativecommons.org/licenses/by/4.0).[128] Copyright 2020, The Authors, published by Springer Nature.

PEDOT:PSS/Au electrode array than for an Au-only electrode array. The electrode with high resolution equivalent to the size of a single neuron (10 × 10 μm electrode surface area and 30-μm interelectrode distance) measured the LFP and action potentials of putative single neurons of epilepsy patients on the human brain surface without invasive penetration by an electrode (Figure 6c).

A stretchable neural interface that has low elastic modulus can provide better contact with the brain and more-stable mechanical properties than ultrathin and flexible neural interfaces, even though they can make conformal contact with the brain surface. The stretchable CP nanowires (PPy-NWs) electrode was fabricated using prestretching methods (Figure 6d); it had a low elastic modulus of ≈450 kPa and high stretchability (up to 100% strain) (Figure 6e).[127] In addition, the structure in which the NWs were embedded in the elastomer substrate (poly(dimethylsiloxane); PDMS) had strengthened adhesion between the electrode arrays and substrate (≈1.9 MPa), so the electrode did not peel off the substrate. The electrode showed negligible resistance change even under 100% tensile strain and after stretching 10 000 times. A stretchable four-channel MEA neural interface was implanted in the visual cortex of epileptic mice and successfully measured brain signals in vivo (Figure 6f).

On the skin, soft electrodes also obtain better electrophysiological signals than conventional metal electrodes do. Ag/AgCl wet electrodes that form low impedance with the scalp through conductive gel and have outstanding SNR are typical noninvasive electrodes used for EEG measurement.[129] However, use of them for high-density EEG measurement is difficult because gel leakage can form a short circuit between adjacent electrodes[128] and because slow drying of the conductive gel induces impedance change during measurement.[130] Dry electrodes that may overcome the shortages of wet electrodes have been reported to measure electrophysiological signals on the skin without conductive gel.[131] An ultrathin-film dry electrode has better skin contact and lower skin/electrode impedance than traditional dry electrodes, but when it is worn for a long time, perspiration can reduce the reliability of skin contact and change the impedance between electrode and skin.[132]

To solve this problem, ultrathin tattoo electrodes composed of CP and fabricated by inkjet-printing have been suggested.[128] They can form conformal and imperceptible contact with the scalp, and impedance between electrode and skin is constant because sweat does not begin to accumulate for a long time (Figure 6g). The tattoo electrode successfully measured changes in alpha waves on the scalp of the human occipital lobe during resting and waking stages. Compared with medical-grade Ag/AgCl electrodes, the tattoo electrode showed similar time-frequency plots and power spectral density, but higher sensitivity to neural noise (Figure 6h). In addition, in EEG/magnetoencephalography recording, which can precisely analyze brain activity with high temporal resolution by simultaneously measuring changes in electric and magnetic fields in the same neuron area, the metal electrodes interfered with magnetic fields and generate artifacts, but the metal-free tattoo electrode measured the signal without interfering.

3.1.2. Hydrogels

Biocompatible hydrogels have an elastic modulus similar to that of soft tissue (≈10 kPa), so intimate cellular integration is possible.[47] Alginate hydrogel was used as a buffer coating to offset the mechanical mismatch between stiff invasive neural electrodes and soft brain tissue (**Figure 7**a).[133] The SNR were significantly lowered when the hydrogel was coated on the metal electrode; this decrease may occur because the hydration induced swelling of the hydrogel and thereby increased the distance between the electrodes and neurons (Figure 7b). In contrast, when the hydrogel was coated on a metal electrode that had been coated with PEDOT, the degradation of SNR was reduced because the low impedance of PEDOT decreased the noise level of the neural signal (Figure 7b).

PVA hydrogel has been used as a substrate with fully embedded soft electrodes (PEDOT-modified carbon fabric (PEDOT-CF)) (Figure 7c).[134] PVA does not change in size during gelation as the electrode is embedded, so strain mismatch with the electrode is avoided; as a result, the substrate was not deformed. In addition, the ion conductivity and oxygen diffusivity of PVA are similar to those of saline solution. Therefore, implanted PVA hydrogel can permit circulation of tissue fluids containing oxygen and nutrients; this is an advantage over ultrathin conformable electrodes that use plastic film, which are impermeable to body fluids. The comparable stiffness (≈10 kPa) of the PVA hydrogel to that of living tissues, adhesiveness to the brain surface, and hydrophilic nature made the hydrogel electrode superior to commercially available ECoG electrodes that use silicon, which slip on the wet surface due to their hydrophobic nature and incomplete edge contact to the curved brain surface (Figure 7d).

A PEDOT-CF/hydrogel electrode has a lower impedance in the frequency region (<1 kHz) of brain signals and higher capacitance (70 mF cm^{-2}) than conventional metal electrodes (0.15 mF cm^{-2}), and therefore have higher SNR than metal electrodes in the power spectrum of in vivo rat brain epileptic waves (Figure 7d).[134] When stimulated by a radio-frequency current, metal electrodes are affected by induction heating and can increase in temperature to levels that can damage brain tissue during simultaneous ECoG-fMRI measurement; the totally organic soft electrodes do not have this problem.

Freestanding CP hydrogel composites with biocompatibility, conformability, and stability have been used as electrodes for transcranial electrical stimulation (TES) and recording of brain activity.[135] An aloe vera hydrogel/PEDOT:PSS composite electrode simultaneously induced focal seizures and acquired the evoked neural activity on the rough surface of the skull of rat. The freestanding TES CP hydrogel film attached to the skull surface absorbed water at the interface and became hydrated and softened, and therefore developed mechanically conformal contact with the rough and porous surface of the skull (Figure 7e). The CP hydrogel film that showed lower in vivo electrochemical impedance and higher charge capacity than conventional metal TES electrodes (Figure 7f), stimulated epileptic activity of neurons and recorded neurophysiological signals (Figure 7g).
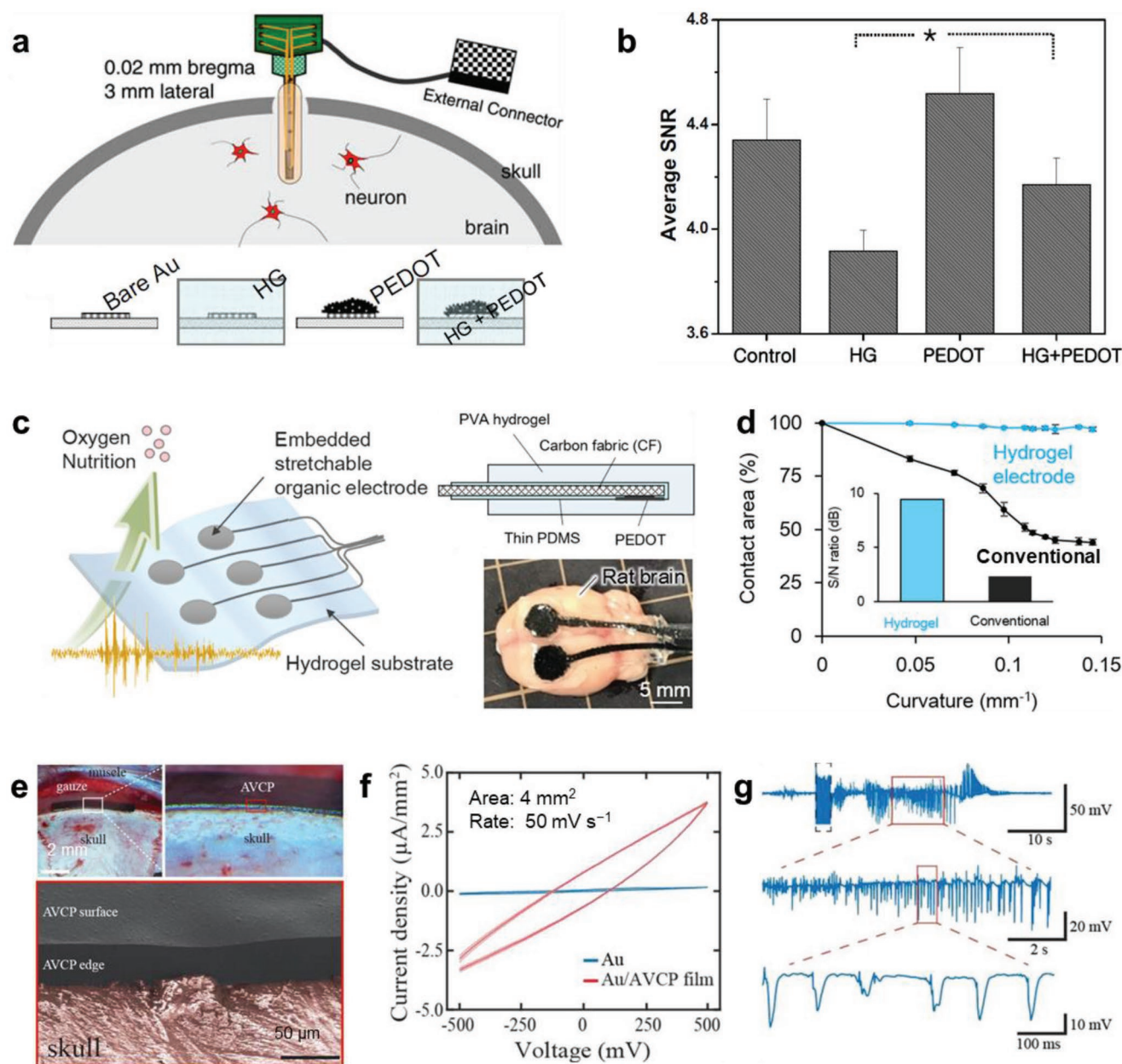
Figure 7. Hydrogel neural interfaces for brain signal recordings. a) Schematics of brain-implanted electrodes with bare Au, Au coated with hydrogel (HG), PEDOT, and HG + PEDOT. b) SNRs recorded at a 1.5 mm depth in the auditory cortex from electrodes, including an Au electrode without modification (control) and after modification with HG, PEDOT, and HG + PEDOT. a,b) Reproduced with permission.[133] Copyright 2010, Elsevier. c) Schematic of PVA hydrogel–PEDOT–carbon fiber (CF) composite subdural electrode. Digital image of hydrogel electrode placed on an extracted and rat brain. d) Contact area of the hydrogel electrode and a conventional electrode on the curved surface. Inset: SNR of in vivo rat brain epileptic wave measurement. c,d) Reproduced under the terms of the CC-BY Creative Commons Attribution 4.0 International license (https://creativecommons.org/licenses/by/4.0).[134] Copyright 2019, The Authors, published by Springer Nature. e) Optical microscopy and scanning microscopy images of aloe vera hydrogel/PEDOT:PSS (AVCP) film conforming to a rat skull. f) In vivo cyclic voltammetry of Au and Au/AVCP films. g) Intraoperative epileptic seizure induced and recorded by AVCP TES electrodes on a rat skull. e–g) Reproduced with permission.[135] Copyright 2019, Wiley-VCH.

3.1.3. Organic Electrochemical Transistors

Although surface electrodes that use CP can read electrophysiological signals, OECTs that use CPs as channels can provide high SNR by applying a built-in local pre-amplification system.[136–139] With a structure similar to a neurogrid, 17 OECT array neural interfaces composed of PEDOT:PSS channels and Au source drain electrodes between 2 μm-thick parylene C films were formed by photolithography (**Figure 8**a). In addition, a PEDOT surface electrode was formed next to the OECT, and an sEEG silicon probe with a linear array of Ir electrodes was inserted into the hole at the center of the array to compare
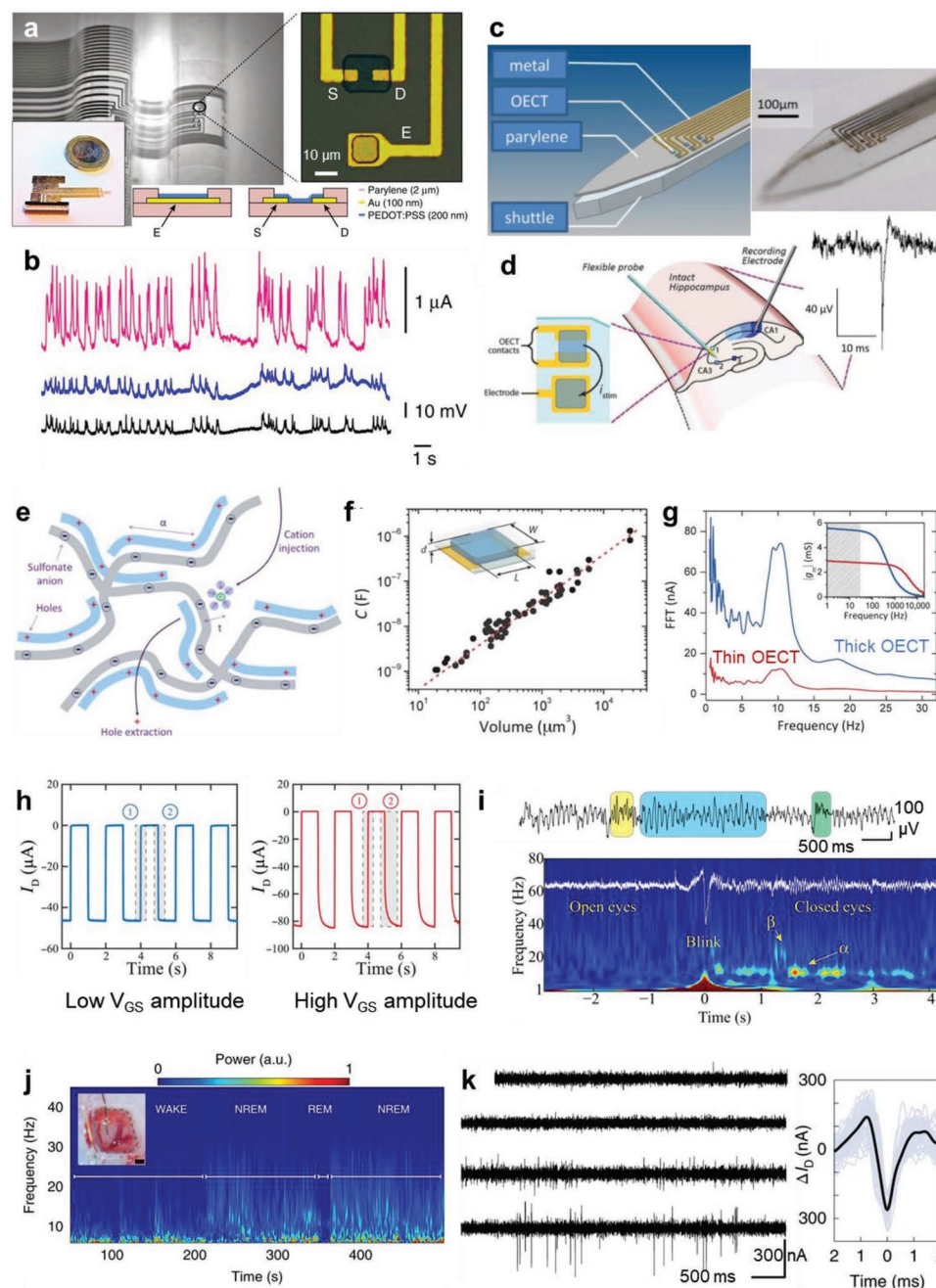
Figure 8. OECT neural interfaces for brain signal recordings. a) Microscopy and schematic images of the probe with OECT and organic electrochemical electrodes array (S: source, D: drain, E: electrode). b) Recorded signals from an OECT (pink), a PEDOT:PSS electrode (blue), and an Ir-penetrating electrode (black). a,b) Reproduced with permission.[136] Copyright 2013, The Authors, published by Springer Nature. c) Schematic and microscopy images of OECT probe with and SU-8 shuttle. d) Schematic image of stimulating pyramidal neurons in intact hippocampal preparations with OECT probes and recorded action potential when section of CA3 was stimulated. c,d) Reproduced with permission.[74] Copyright 2015, Wiley-VCH. e) Schematic of dedoping of PEDOT:PSS caused by ion injection (a: average site distance). Reproduced with permission.[140] Copyright 2016, Wiley-VCH. f) Volumetric capacitance of PEDOT:PSS. g) Fast Fourier transform analysis of EEG recordings (inset: transconductance frequency response). f,g) Reproduced with permission.[141] Copyright 2016, The Authors, published by AAAS. From ref. [141]. © The Authors, some rights reserved; exclusive licensee AAAS. Distributed under a CC BY-NC 4.0 license http://creativecommons.org/licenses/by-nc/4.0/. Reprinted with permission from AAAS. h) Temporal response of the drain current (I_D) with a symmetrical rise (dedoping, 1) and fall (doping, 2) in response to pulsed gate voltage input. Asymmetric temporal response of I_D with longer doping time than dedoping time. i) Recordings and time-frequency spectrogram of μ-EEG IGT. h,i) Reproduced with permission.[142] Copyright 2019, The Authors, published by AAAS. j) Time–frequency spectrogram of chronic LFP recording from a cortical surface. k) High-pass filtered traces (250–2500 Hz) showing neural action potential recorded from four e-IGTs in deep layers of rat cortex. Trigger averaging of waveforms with consistent action potential morphology. j,k) Reproduced with permission.[143] Copyright 2020, The Authors, published by Springer Nature.

**ADVANCED
SCIENCE NEWS**

www.advancedsciencenews.com

**ADVANCED
MATERIALS**

www.advmat.de

the measured signals recorded from three types of electrodes. OECT obtained a higher SNR than the PEDOT surface electrode during the measurement of the same signals from the same neurons (Figure 8b). OECT also measured signals with superior SNR compared to penetrating silicon probes, even though they measured signals from different depths (Figure 8b).

A 4 µm-thick penetrating probe with CP OECTs stimulated individual neurons at specific locations inside the brain and recorded neural signals (Figure 8c).[74] Rigid thick probes that use silicon may damage soft tissues, and the recording interface may deteriorate due to foreign-body effects and inflammatory reactions. The ultrathin organic neural probe can minimize the side effects caused by mechanical mismatch. CP OECT and surface electrodes embedded in a 4 µm-thick parylene C substrate were implanted into the brain by an SU-8 shuttle. Unlike silicon probes, organic probes did not show side effects such as glial scar formation even 1 month after implantation into the cortex of mice. OECT electrodes implanted in a completely extracted and intact hippocampus evoked local network and single cell response when monophasic current pulses were applied to CA3 pyramidal neurons in the hippocampus (Figure 8d).

The high charge capacity of CPs is a result of the volumetric capacitance induced by their uptake of ions in the electrolyte (Figure 8e).[140,141] The capacitance per unit volume of $C^* = 39.3 \pm 1.3$ F cm^{-3} varies linearly according to the volume (length, width, and thickness) of the CP (Figure 8f). At a thickness of about 130 nm, the capacitance per unit area of OECT was calculated to be 500 µF cm^{-2}, which is 100 times higher than that from double-layer capacitance (5 µF cm^{-2}) of the more-traditional electrolyte-gated OFETs (EGFETs) structure that only uses an EDL.[140,141] In an OECT that had a low driving voltage, in which ions penetrate from electrolyte to the CP without significant ion accumulation at the surface of CP (i.e., negligible ion injection barrier), the transconductance increased as the volume of the CP increased. Therefore, an OECT that had a thick channel in the same area had about twice the transconductance of a thin-channel OECT (with fixed channel width and length, and different thickness 230 vs 870 nm), so EEG signal detection improved (Figure 8g).

An internal ion-gated OECT (IGT) uses mobile ions embedded inside a CP, and does not exchange ions with an external electrolyte, so each transistor can be gated individually.[142] Also, an IGT has high transconductance and high speed because of its high volumetric capacitance and the short transit time of mobile ions in a CP. D-Sorbitol, which is a biocompatible hydrophilic sugar alcohol that uptakes water molecules, was used with PEDOT:PSS. The addition of D-sorbitol forms an ion reservoir to facilitate the movement of ions in the channel, and elongates the PEDOT-rich domain to improve the conductivity of PEDOT:PSS. In addition, between the gate electrode and the channel, chitosan, which selectively conducts ions but not electrons, was formed as an ionic membrane. In the device, internal ions moved to the external electrolyte when gate-source voltage V_{GS} pulse amplitude was high (0.9 V), but not under normal driving conditions (e.g., V_{GS} pulse amplitude = 0.4 V) (Figure 8h). The doping/dedoping process of IGT is faster (time constant = 32.30 µs) than conventional EGFETs and OECTs. IGT also has high transconductance (maximum 32.30 mS)

as a result of the volumetric capacitance. The ultrasmall IGT with a light weight and conformable structure could contact the skin without additional chemicals, and did not induce redness or irritation on the skin even after long-time use; these abilities are superior to those of large rigid metal EEG electrodes that require an ionic conducting gel and strong chemical adhesive. In addition, even on the scalp, where EEG was measured, the ultrasmall IGT (50 × 100 µm channels in a 1.5 mm-wide ribbon) was easily attached between hairs and showed excellent mechanical and electrical stability. The attached IGT recorded clearly the posterior dominant rhythm, an 8 to 12 Hz (alpha-wave) oscillation following eye blinking (Figure 8i).

Most OECTs that use PEDOT:PSS operate in a depletion mode that lowers the conductivity by reducing PEDOT:PSS to PEDOT^0 with a positive voltage (normally ON), but most electronic devices operate in an enhancement mode, so to achieve compatibility with the other electronic systems, an OECT that works in enhancement mode is desirable. A poly(ethylene imine) (PEI) layer was added to the depletion-mode IGT (channel: PEDOT:PSS, ion reservoir: D-sorbitol, and ion membrane: chitosan), to reduce PEDOT:PSS to PEDOT^0 and form PEI:PSS ionic bonds by transferring electrons during the OFF state.[143] In the ON state, PEI$^+$ and PSS$^-$ were released by application of negative voltage; they formed PEDOT$^+$:PSS$^-$, so that an enhancement-mode IGT (e-IGT) with increased conductivity was fabricated. The e-IGT had a fast rise time of 2.9 µs, and therefore could record neural signals from the cortical surface and deep cortical layers of freely moving rats. The e-IGT array located on the cortical surface recorded high-quality LFP signals during non-rapid eye movement sleep, rapid eye movement sleep, and wakefulness (Figure 8j). In addition, e-IGT electrodes inserted into deep cortical layers could record the spiking activity of individual neurons in vivo (Figure 8k).

3.2. Neural Interfaces for Cardiac Signals

A beating heart moves continuously. Cardiac interface electrodes are deformed by this movement, so mechanical stretchability is important to enable stable detection of cardiac signals. In addition, a high-resolution electrophysiological mapping electrode array is required for accurate diagnosis and treatment of cardiac diseases such as chronic arrhythmias. Conventional catheters find causes of the arrhythmia inside the atrium, but have a low spatial resolution and cannot map outside the heart. A high-density cardiac interface electrode that uses hydrogel and that is placed on the outer membrane of the heart can conduct in vivo electrophysiological mapping at the cellular level in real-time.[144] An intrinsically stretchable and tissue-level soft Au/PEDOT:PSS conducting hydrogel electrode was encapsulated by diacrylate-modified perfluoropolyether (PFPE-DMA) insulating elastomer. The electrode was fabricated by photolithographic microfabrication with sub-100 µm resolution comparable to the size of a single cardiomyocyte, then manufactured in a large area (100 cm^2) (**Figure 9**a). Electrodes formed robust and intimate tissue coupling with cardiac cells of rabbits and pigs during the cardiac cycle while stably maintaining chemical, mechanical, and electrical properties. Pathological abnormalities were identified with fine temporal resolution and cell-level
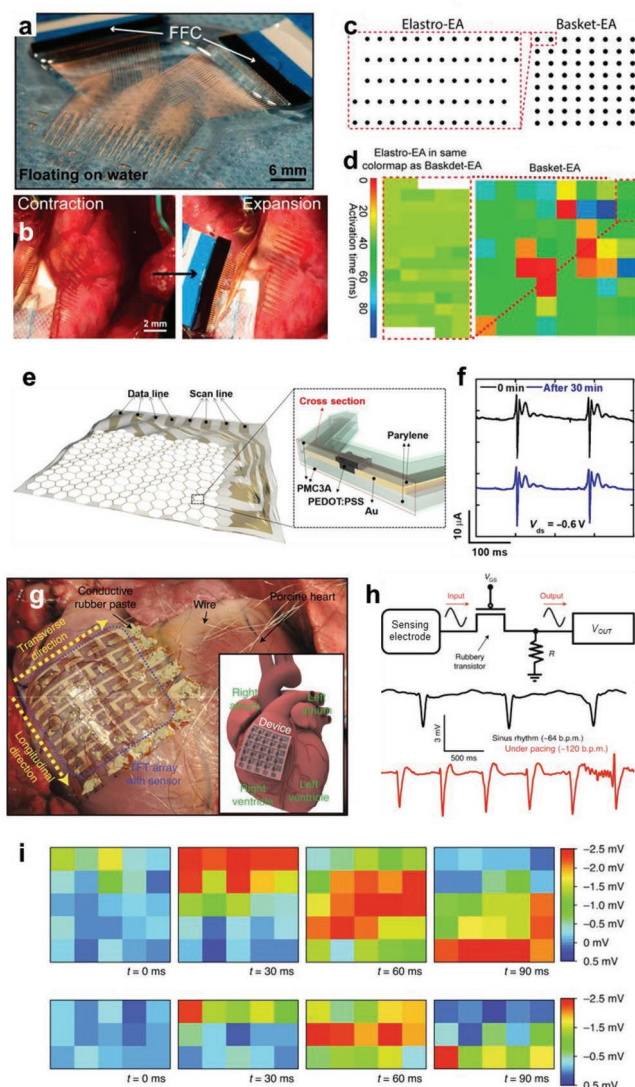
**ADVANCED
SCIENCE NEWS**

www.advancedsciencenews.com

**ADVANCED
MATERIALS**

www.advmat.de

Figure 9. Organic neural interfaces for cardiac signal recordings. a) Digital image of intrinsically stretchable and tissue-level soft Au/PEDOT:PSS conducting hydrogel electrode array. b) Digital images of pig right atrium during a contraction–expansion cycle. c) Relative positions of high-spatial-resolution epicardial elastro-electrode array (EA) and endocardial basket electrodes. d) Isochronal maps of activation time from the epicardial elastro-EA (left) and endocardial basket electrodes (right). a–d) Reproduced with permission.[144] Copyright 2020, The Authors, published by National Academy of Sciences, USA. e) Schematic images of stretchable OECT array on honeycomb grid substrate. f) Recorded ECG by stretchable OECT array with PMC3A coating for 30 min. e,f) Reproduced with permission.[145] Copyright 2018, The Authors, published by AAAS. From ref. [145]. © The Authors, some rights reserved; exclusive licensee AAAS. Distributed under a CC BY-NC 4.0 license http://creativecommons.org/licenses/by-nc/4.0/. Reprinted with permission from AAAS. g) Digital image of a fully rubbery-transistor active matrix on a porcine heart (TFT: thin film transistor). h) Circuit diagram of the sensing system ($R = 100\,k\Omega$). Signals recorded from the electrode array with and without pacing. i) Spatiotemporal electrophysiological signal mapping from 5×5 sensing nodes (upper) and during pacing by the first two rows of the devices (lower). g–i) Reproduced with permission.[146] Copyright 2020, The Authors, published by Springer Nature.

spatial resolution in an animal model of chronic atrial fibrillation. The flexible but non-stretchable cardiac interface was torn by the rabbit's rapid heartbeat (120–150 min^{-1}), but the stretchable hydrogel electrode remained stable without changing its position (Figure 9b). During simultaneous measurement of commercial endocardial-mapping techniques and epicardial recording, the hydrogel electrode had double the atrial-to-ventricular signal ratio and more than 100 times finer spatial resolution than the conventional catheter electrodes, and therefore monitored fine patterns of localized electrical heterogeneity that low-resolution electrodes cannot detect (Figure 9c,d).

The active MEA that uses an OECT array can obtain ECG signals with high SNR by exploiting local signal amplification. Although the existing ultrathin high-resolution MEA built on plastic film is flexible, it has only a limited ability to flex during the dynamic movements of the heartbeat; as a result, platelets can aggregate on the device and form blood clots. Therefore, a 1.2 µm-thick ultrathin flexible parylene film was processed to form a stretchable honeycomb grid-structured substrate (Figure 9e).[145] A 4×4 active OECT array cardiac interface electrode was demonstrated on this substrate. In addition, a 100 nm-thick poly(3-methoxypropyl acrylate) (PMC3A) coating inhibited the formation of a blood clot while maintaining ionic conductivity. A 2.6 µm-thick OECT MEA measured ECG signals on the surface of the heart of rats with high SNR (51 dB) and was not affected by artifact noise caused by heart motion. The sensitivity was not degraded by blood clot formation even after 30 min of measurement (Figure 9f). The spatiotemporal distribution of ECGs on the cardiac surface was recorded using a 4×4 active matrix OECT array as a cardiac interface that covers the right and left ventricular regions.

An ion gel-based 5×5 stretchable active-matrix transistor array, strain and temperature sensors, therapeutic devices (electrical pacing and thermal ablation), and a mechanoelectrical transducer form a 400 µm-thick stretchable epicardial bioelectronic patch (Figure 9g).[146] It was transplanted into an in vivo pig heart. AgNW-embedded PDMS (AgNWs/PDMS) electrodes, poly(3-hexylthiophene-2,5-diyl) nanofibrils (P3HT-NFs)/PDMS blended semiconductors, ion-gel dielectrics, and individual sensing electrodes formed intrinsically stretchable ion-gel-gated organic transistors for spatiotemporal ECG signal mapping (Figure 9h,i).[146] A strain sensor with high gauge factor (7.76) constructed using AuNPs–AgNWs/PDMS and P3HT-NFs/PDMS as the electrode and sensing material can detect the systolic and diastolic strains of the heart at the epicardium for diagnosis of cardiac disorders such as myocardial ischemia. A stretchable temperature sensor composed of AgNWs/PDMS for detecting arrhythmias had linear normalized thermoresistive characteristics in the range of 27–45 °C. The sensing property was independent of the mechanical stretching to 30% strain.

The thermoresistive device also has Joule heating characteristics when a large DC current flows through it. The localized Joule heating increased temperature to ≈68 °C when 3.5 V DC bias was applied, so the device can be used for thermal ablation to destroy tissues that are behaving abnormally. Mechano-electrical transducers made of two thin AgNWs/PDMS electrodes with a thin spacer generated electricity during motion by exploiting the triboelectric effect. The open circuit voltage

**ADVANCED
SCIENCE NEWS**

www.advancedsciencenews.com

**ADVANCED
MATERIALS**

www.advmat.de

and short circuit current were under the normal sinus rhythm (at ≈65 beat per min) 0.68 ± 0.03 V and 8.01 ± 1.17 nA, respectively. After further optimization, they have the potential to harvest energy from the heartbeat as a source of power for sustainable operation of epicardial devices.

3.3. Neural Interfaces for Motor Signals

Interfaces with muscles or motor nerves require higher mechanical stability and adhesion than interfaces with the heart, because the limbs and muscles move irregularly and often contract strongly and abruptly. Electrodes that use hydrogel can meet mechanical requirements with tissue-like softness and stretchability. Moreover, because an action potential in biology is based on ion conduction, an ionic current is converted to an electric current at the electrode/electrolyte interface, but the conversion is greatly affected by the interface impedance. Ion-conductive electrodes can exclude the conversion between the electric current and the ionic current at the biological interface, and therefore can avoid a large voltage drop caused by interfacial impedance. In addition, the ion-conductive electrode is a safe interface that prevents damage to cells that can be caused by local heating, pH change, and electrode corrosion caused by voltage drop and electrochemical reaction at the interface where the conventional electronic conductive electrode directly contacts the cell. An aqueous two-phase system was used to prepare a programmable hydrogel ionic circuit in which a salt solution (highly ion-conductive) is embedded in PEG hydrogel matrices (weakly ion conductive), and then the circuit was applied as a muscle interface (**Figure 10**a).[147] The hydrogel ionic circuit interfaces demonstrated in vivo electrical stimulation of skeletal muscle tissue (Figure 10b). A pair of hydrogel ionic stimulator electrodes was interfaced with a rat's tibialis anterior muscle, then the twitch and tetanic forces of muscles were stimulated by hydrogel or conventional metal electrode and were measured. Twitch contraction was stimulated using a frequency of 1 Hz, and tetanic contraction was stimulated using a frequency of 50 Hz. Generally, smaller amplitude of voltage pulses was required to induce similar contraction force with hydrogel electrodes than with metal electrodes (Figure 10c,d). The results indicate that the hydrogel ionic stimulator is more efficient than standard metal electrodes to transfer electrical signals to skeletal muscle tissue and induce muscle contraction.

A electrically conductive hydrogel composed of PEDOT:PSS increased the low electrical conductivity of the pure ionic hydrogels, and showed high electrical conductivity (47.4 ± 1.2 S cm^{-1}) and low elastic modulus (≈32 kPa).[106] The PEDOT:PSS hydrogel was patterned to a size of 20 µm by using photolithography, then used as an interface with a sciatic nerve (Figure 10e). A UV-crosslinked elastomer insulator composed of PFPE-DMA monomers was coated as stretchable encapsulation (<30 kPa) to reduce leakage current. In long-term in vivo implantation by wrapping neural interfaces around sciatic nerves of mice, conventional flexible plastic cuff electrodes had mechanical mismatch with the tissue, and this mismatch significantly reduced the number of neurofilaments and induced growth of inflammatory tissue at wrapped regions, whereas micropatterned electrically conductive hydrogel electrodes minimized such immune responses.

A neural interface that uses PEDOT:PSS and in which the electrodes and interconnects are composed of electrically conductive hydrogel, has high electric-ionic mixed conductance and lower interface impedance than the conventional neural interfaces of the PEDOT:PSS-coated gold electrode, hydrogel-coated gold electrode, platinum electrode, and a pure ionic conductor (Dulbecco's modified eagle's medium [DMEM], which is a widely used cell-culture medium).[106] In addition, the electrically conductive hydrogel has a higher volumetric capacitance (9800 µF cm^{-3}) than PEDOT:PSS (2200 µF cm^{-3}), and higher current density (1359 mA cm^{-2}) than DMEM (1 mA cm^{-2}), platinum (48 mA cm^{-2}), PEDOT:PSS (60 mA cm^{-2}), and PANI (80 mA cm^{-2}) under a bipolar pulsed voltage of 0.5 V at 50 Hz (Figure 10f). Therefore, the conductive hydrogel electrode can deliver a high current density of 10 mA cm^{-2} with a small voltage of 50 mV to induce leg movement, whereas conventional Pt electrodes require at least 500 mV. Therefore, the conductive hydrogel electrode induced a larger leg movement at a low voltage, than the Pt electrodes did (Figure 10g).

The growth of organs and nerves further exacerbates the mechanical mismatch with rigid neural interfaces. Therefore, implanted electronic devices must be replaced periodically. However, growth-adaptive morphing electronic devices reduce the mismatch at the interface between the electronic device and the growing cell, and thereby reduce the occurrence of problems such as displacement of electrodes, weakening of adhesion, and inhibition of cell growth due to mechanical pressure (Figure 10h).[148] Growth of the body proceeds very slowly, compared to dynamic movements. Therefore, the morphing electronic devices must have viscoplastic properties that can adapt to slow growth, rather than the viscoelastic properties of existing stretchable neural interfaces that maintain their abilities during dynamic motion.

A viscoplastic PEDOT:PSS/glycerol conductor has 3.9 times more elongation than pristine PEDOT:PSS at 100% strain (Figure 10i).[148] Also a self-healable viscoplastic polymer, isophorone bisurea (IU)-PDMS-4,4'-methylenebis(phenyl urea) (MPU) (PDMS–IU0.6–MPU0.4) film underwent irreversible plastic deformation at 100% elongation. PEDOT:PSS/glycerol/viscoplastic polymer had viscoelastic properties at elongation speed >5% s^{-1}, but showed zero stress at elongation speed <0.05% s^{-1}, so this combination does not cause mechanical mismatch as the nerve grows.

The self-healing properties of the substrate enable a biomechanically compatible, suture-free, and individually reconfigurable interface of the sciatic nerve with soft morphing electronics (MorphE). MorphE wrapped around the sciatic nerve, made a robust neural interface by simply attaching both sides to form a soft enclosure (Figure 10j).[148] The PEDOT:PSS/glycerol strain sensor that constituted MorphE measured the increase in the diameter of the sciatic nerve from 0 to 4 weeks post implantation, and obtained results similar to the change in the actual nerve diameter. MorphE showed stable neuromodulation, but a conventional cuff electrode (platinum/PDMS) became partially detached due to nerve growth 2 weeks after implantation, and therefore ceased to evoke detectable compound action potential. Additionally, conduction velocities were similar in MorphE-implanted mice and nonimplanted mice from week 0 to 8 post-implantation (Figure 10k). The implanted mice exhibited normal gait, sensory
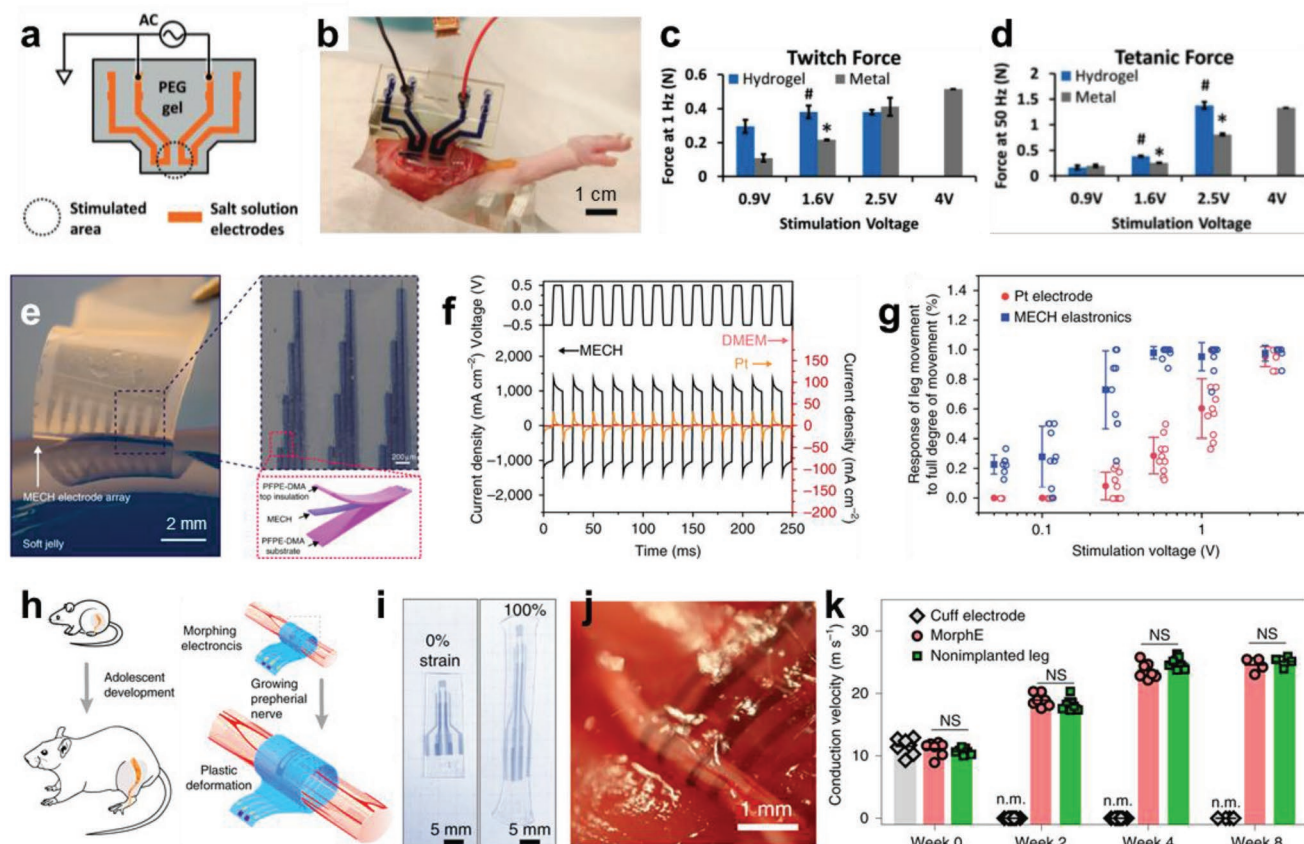
Figure 10. Organic neural interfaces for motor signal recordings. a) Schematic image of hydrogel ionic simulator circuit. b) Digital image of hydrogel ionic simulator placed on rat *tibialis anterior* (TA) muscle. c,d) Force of TA muscle stimulated with 1 Hz (c) and 50 Hz (d) pulsed signals to induce twitching and tetanus, respectively. a–d) Reproduced with permission.[147] Copyright 2018, Wiley-VCH. e) Digital images of PEDOT:PSS micropatterned electrically conductive hydrogel (MECH) electrode array. f) Current densities of MECH, platinum, and DMEM. g) The response of leg movement to the full degree of movement (%) with different stimulation voltages for the MECH and platinum electrodes. e–g) Reproduced with permission.[106] Copyright 2019, The Authors, published by Springer Nature. h) Schematic images of adolescent development of the rat and the MorphE that conformally adapts to sciatic nerve growth. i,j) Digital images of MorphE under 0% and 100% strain (i) and wrapped around the sciatic nerve (j). k) Conduction velocity measured by MorphE, cuff electrodes, and nonimplanted nerve in growing rats (n.m., not measurable due to device failure). h–k) Reproduced with permission.[148] Copyright 2020, The Authors, published by Springer Nature.

function, motor responses, and minimal structural and histological changes. These results indicate that MorphE adapts adequately to nerve growth.

3.4. Neural Interface for Optogenetics

Organic neural electrodes were applied to record neural signals that were artificially triggered by optical stimulation. Optogenetics is a biological technology that can use light to control ion channels of nerves in living cells.[149,150] A light-sensitive gene (e.g., channelrhodopsin [ChR]) implanted in the target cell can be exploited to control neural activities of the cell with high spatiotemporal accuracy. In mice genetically modified with ChR for the motor nerves and their terminals in the hind limbs, the muscle was activated by a laser beam with a wavelength of 473 nm, and EMG signals were evoked (**Figure 11**a).[151] To record the EMG signal, a 2 μm-thick, 5 × 5 array of active matrix neural electrodes integrated with OECTs and OFETs was laminated on the surface of the gracilis

muscle. OECTs that use PEDOT:PSS with high transconductance can read signals while in contact with the tissue surface, and OFETs that use dinaphtho[2,3-b:2′,3′-f]thieno[3,2-b]thiophene (DNTT) can switch the OECT on and off with a high on/off current ratio. The integrated OECT-OFET neural electrode had a cutoff frequency of 3 kHz, a transconductance of >1 mS, an output sinusoidal signal of 50 μA, and a delay of only 48 μs at an input of a sinusoidal signal of 3 kHz with an amplitude of 50 mV (Figure 11b). Also, after crumpling, the OFET showed only 1% change in "on" current and 5% change in "off" current, and no change in transconductance of OECT. Because of a fast response rate, the EMG signal evoked by the rat's gracilis muscle surface of the leg moved by light was recorded with high temporal resolution of milliseconds (Figure 11c). The 2 × 2 neural electrode array mapped the spatial distribution of signals; these electrical and mechanical properties support the suitability of such arrays as bioelectrodes.

Transparent nerve electrodes can increase the efficiency of nerve cell stimulation by light. For electronic materials that have electrical signals that can be changed by photoexcitation,
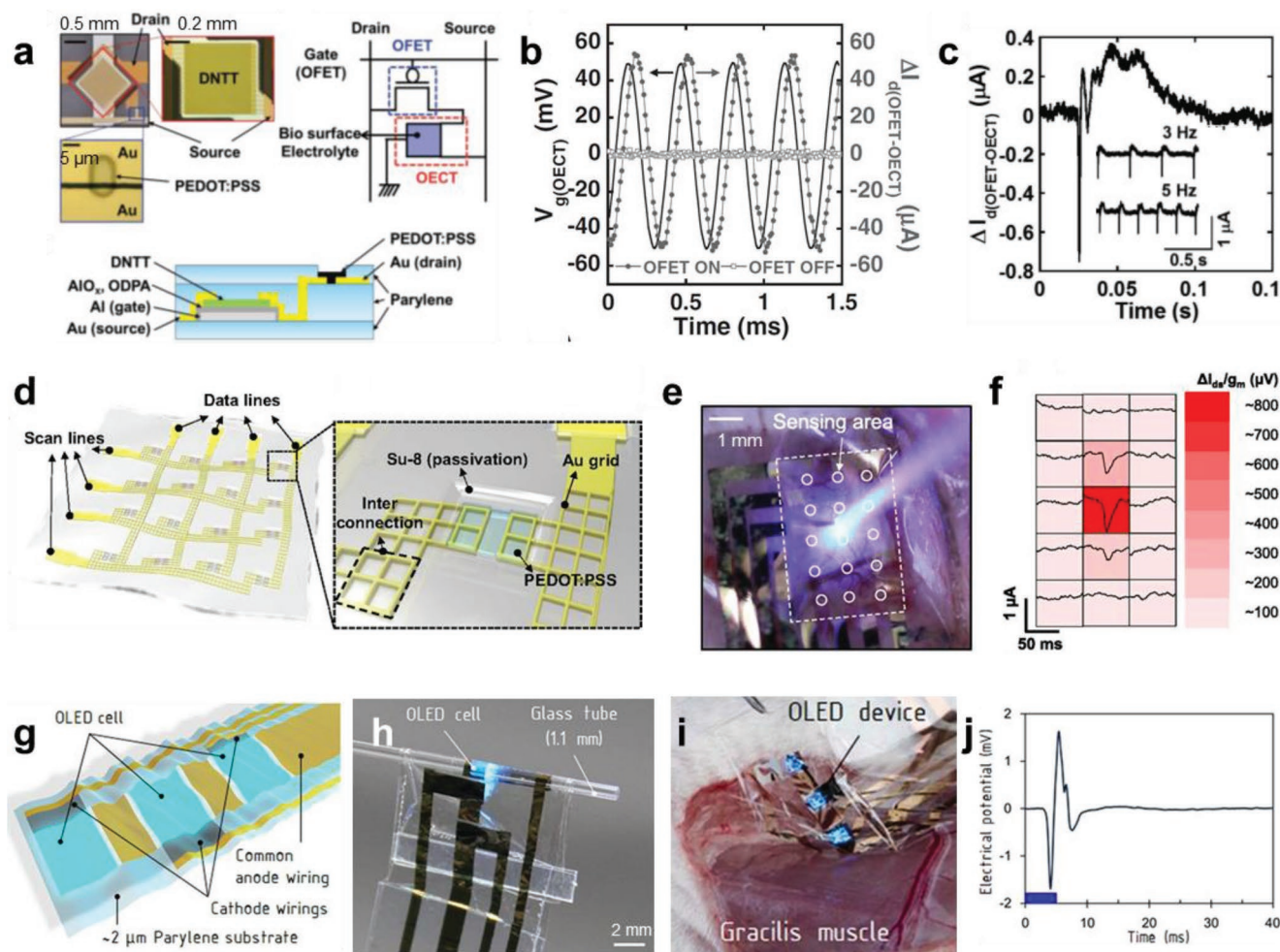
Figure 11. Organic neural interfaces with optogenetics. a) Microscopy and schematic images of a sensing pixel integrated with OFET and OECT. b) I_d–time curve of 3-kHz oscillation with $V_g = \pm 50$ mV when the OFET was ON and OFF. c) Action potential evoked by a laser flash (inset: I_d–time curve with 2, 3 or, 5 Hz stimulation). a–c) Reproduced with permission.[151] Copyright 2016, Wiley-VCH. d) Schematic images of transparent electrophysiology OECTs array. e,f) Digital image (e) and spatial mapping of the brain signal (f) of 3 × 5 transparent electrophysiology array on the cortical surface of optogenetic mice with blue laser stimulation. d–f) Reproduced with permission.[152] Copyright 2017, The Authors, published by National Academy of Sciences, USA. g–i) Schematic (g) and digital images of ultraflexible OLED device under bending (h) and placed on gracilis muscle (i). j) EMG evoked by ultraflexible OLED device. g–j) Reproduced with permission.[153] Copyright 2020, The Authors, published by National Academy of Sciences, USA.

illumination artifacts can cause problems in measurement accuracy, so conductive materials that are not photosensitive are required. A 3 µm-thick 3 × 5 transparent neural electrode composed of OECT that uses PEDOT:PSS and Au grid electrode was conformal and transparent on the surface of a rabbit brain (Figure 11d).[152] The optimized Au grid electrode patterned with a line width of 3 µm and an interval of 18 µm had a transmittance of 69% and a sheet resistance of 3 Ω sq^{-1}. When transferred to the 100% pre-strained substrate, Au grid electrode had a sheet resistance of 7 Ω sq^{-1} even at 50% compressive strain. On the surface of the rat brain that had been modified to express ChR, at light intensity of 40 mW, OECT neural electrodes with transparent Au grid electrodes had twice the amplitude (700 µV) of light-evoked ECoG signals compared to non-transparent OECT neural electrodes that use Au film electrode. In addition, a 3 × 5 array of transparent OECTs with 1 mm^2 spatial resolution mapped light-evoked ECoG signals on the surface of a rat brain (Figure 11e,f).

Nerve-conformal flexible organic light emitting diodes (OLEDs) have also been used as optogenetic stimulators (Figure 11g,h).[153] Flexible OLEDs achieve conformal contact, so they enable optical stimulation of tissues without causing damage, and can emit light over a larger area than point-type light sources (optical-fiber-coupled lasers or inorganic light emitting diodes (LEDs)), enabling the activation of multiple neurons. Although the OLED emits relatively weaker light (0.5 mW mm^{-2}) than inorganic LEDs, it is sufficient to exceed the threshold of nerve excitation (≈0.3 mW mm^{-2}). To stimulate the rat brain and peripheral nerves (genetically modified with ChR (sensitive to light of wavelength $\lambda = 470$ nm)), the OLED emits light of $400 \leq \lambda \leq 580$ nm (peak intensity at 455 nm). Three OLEDs with thickness 2 µm showed mechanical stability even at a bending radius of 50 µm. The genetically modified gracilis muscle or sciatic nerve was stimulated using a conformal flexible OLED light source to contract the gracilis muscle or gastrocnemius muscle, and EMG was measured in each muscle (Figure 11i,j).

The evoked potential was measured in the primary somatosensory cortex (S1) by stimulating sensory nerves in the hind legs by using flexible OLEDs attached to the soles of the feet. A flexible optogenetic stimulator that uses OLEDs could stimulate cells with mechanical stability even during leg movement, and did not damage cells, whereas a 5 mm-long rigid-cuff optical emitter cover around the sciatic nerve damaged the myelin sheaths due to repetitive mechanical stress, by 10 days after implantation.

In addition, the ultrathin OLED made of non-magnetic material proves MRI compatibility by not interfering with the magnetic field and RF field of MRI, whereas an inorganic (GaN) LED has high electrical conductivity and high magnetic permeability, and therefore creates artifacts during MRI measurement.

4. Nervetronics for Neuroprosthetics

Neuroprosthetics are being developed to treat injured nervous systems.[8,22,31,154–158] Various kinds of neuroprosthetics stimulate the nerves mechanically (pressure, vibration) or electrically (DBS, functional stimulation). Electrical stimulation has advantage that it can directly activate neurons. Electrical neuromodulation has increased the diversity of strategies to treat neurological disorders. For example, DBS directly changes the brain activity by administering electrical impulses from a pulse generator. DBS is a common treatment for Parkinson's disease, essential tremor, and dystonia.[159–161] Also, spinal cord stimulators are widely used to alleviate chronic neuropathic pain.[162,163] These neurostimulation strategies provide new ways to improve the quality of life for patients who have neurological disorders. However, these methods have limited abilities to treat patients who have serious problems, such as spinal cord disorder, amputated limbs, and sensorimotor disorders. Therefore, new approaches are needed in neuroprosthetics research to rehabilitate patients who have neural disorders.

Nervetronics are electronic artificial nerves that mimic biological nerves and related neuronal connection. Biomimetic organic bioelectronics may provide next-generation neuroprosthetic applications that exploit neurologically inspired electronics by emulating the biological peripheral nervous system.[31,158,164–173] Especially, use of organic soft nervetronics that can emulate neural signal transmission mechanisms and synaptic plasticity would enable development of next-generation neuroprosthetics that do not use conventional rigid digital computing systems, which consume a large amount of power. In this chapter, we review the principle and achievements in organic nervetronics for neuroprosthetics. We also address the challenges that remain before the neurostimulation strategies can be used clinically.

4.1. Artificial Synapse

Artificial synapses can emulate biological synaptic plasticity (**Figure 12**a), so they are essential elements for nervetronics. The principle, signal transmission, and synaptic plasticity of biological synapse have been widely studied in organic artificial synapses that have two-terminal[174–185] or three-terminal[158,166,171–173,186–203] structures and various working mech-
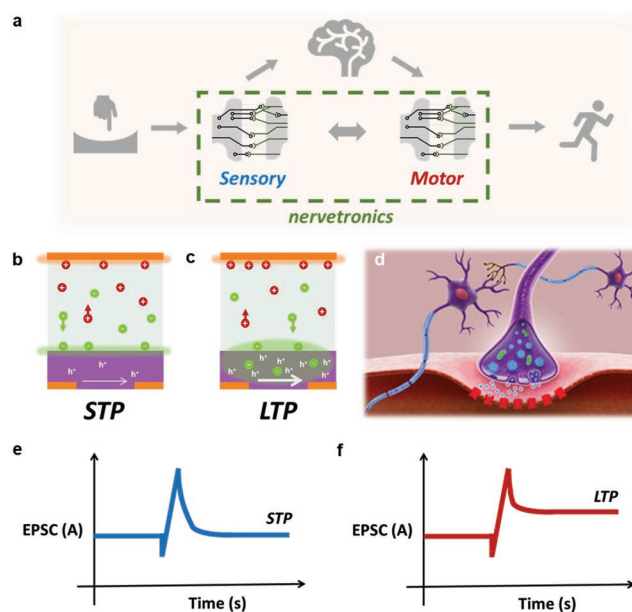

Figure 12. Schematics of the nervetronics and artificial synapses. a) Nervetronics connections with the biological system. b,c) Ion movement of short-term potentiation (STP) (b) and long-term potentiation (LTP) (c). d) Biological synapse and cross section of electrolyte gated transistor-based artificial synapses. e,f) Time verses excited post-synaptic current of STP (e) and LTP (f).

anisms such as charge trapping,[179–181] conductive filament formation,[175–178] ferroelectric tunnel junction,[182,199] ion migration,[183] and electrochemical reaction.[173,189,190,193,194,198,200,201]

Especially, organic artificial synapses that use electrolyte-gated transistors (EGTs), which exploit ion migration and electrochemical reaction, are most-widely adapted as a main part of nervetronics, because decoupled "write" and "read" terminals in the transistor structure can offer more reliable, versatile, and functional operations than two-terminal devices. Moreover, an EGT can form an EDL (10 µF cm^{-2})[204–208] and can have high volumetric capacitance (up to 900 F cm^{-3}) due to ion migration, so adequate charges for operation can be induced by low-voltage inputs.[141,209–212] The ion migration toward the channel also can yield synaptic properties (Figure 12b,c).[169,191,200] This phenomenon is analogous to the biological synaptic mechanism, in which neurotransmitters diffuse through the synaptic cleft in a biological nervous system (Figure 12d). Numerous ion-permeable polymers have been used for state-of-art artificial synapses; examples include conducting polymers such as PEDOT:PSS,[181,188–190,193–195,197,198] and semiconducting polymers that include thiophene-based semicrystalline polymers such as P3HT,[167,170,191,196,200,202] poly(2-(3,3′-bis(2-(2-(2-methoxyethoxy)ethoxy)ethoxy)-[2,2′-bithiophen]-5-yl)thieno[3,2-b]thiophene) (p(g2T-TT)),[187] poly[[4,8-bis[5-(2-ethylhexyl)-2-thienyl]benzo[1,2-b:4,5-b′]dithiophene-2,6-diyl][2-(2-ethyl-1-oxohexyl)thieno[3,4-b]thiophenediyl]] (PBDTTT-C-T),[173] and donor-acceptor polymers such as poly(thienoisoindigo-naphthalene) (PTIIG-NP),[169] and poly[(3,7-bis(heptadecyl)thieno[3,2-b]thieno[2′,3′:4,5]thieno[2,3-d]thiophene-5,5′-diyl)(2,5-bis(8-octyloctadecyl)-3,6-di(thiophen-2-yl)pyrrolo[3,4-c]pyrrole-1,4(2H,5H)-dione-5,5′-diyl)] (FT4-DPP).[31,158,241]

When a positive or negative voltage spike is applied to the gate electrode of the organic synaptic transistor, ions of the same charge as the spike move toward the channel and form an EDL.[191,213] It induces charge carriers in the channel of the transistor, so they are maintained during the EDL formation; this maintenance is the source of short-term synaptic properties (Figure 12b,e). Further, when the ions penetrate the active layer (channel), they contribute to the volumetric capacitance and induce additional charge carriers.[141,210,212] When the ions penetrate the active layer and become trapped in it, the charge carriers can be still induced, even after the transistor is in the OFF state; this trapping is the source of the long-term synaptic properties of artificial synapses (Figure 12c,f).[169,191,200]

For instance, artificial synapses with P3HT–polyethylene oxide (PEO) core–sheath organic nanowire (ONW) showed synaptic responses by the above mechanism.[191] An ion-gel gated synaptic transistor was demonstrated using a 300 × 300 nm ONW channel and an ion gel composed of poly(styrene-*block*-methyl methacrylate-*block*-styrene triblock copolymer and 1-ethyl-3-methylimidazolium bis(trifluoromethyl sulfonyl) imide ([EMIM][TFSI]). Before the voltage spike (pre-synaptic spike) is applied, the anion ([TFSI$^-$]) and cation ([EMIM$^+$]) are distributed randomly in the ion-gel medium. During application of a negative pre-synaptic spike, anions accumulate near the ONW channel. They form the EDL, which induces generation of holes in the ONW. Some anions penetrate the PEO:P3HT and induce additional charge carriers in the ONW. After the pre-synaptic spike ends, the penetrated ions gradually drift back to the ion-gel medium. This release of trapped anions reduces the number of induced charge carriers in the ONW, and results in the synaptic-decay response.

Artificial synapses have been widely studied for use to modulate the diverse functions of the biological nervous system. Biological nerves have properties that are suited for numerous uses (learning and memory, sensing, neural-signal integration), so fields of study of artificial synapses have been developed to fit their performance to each situation. For instance, artificial synapses with conductive PEDOT:PSS have emulated the ability of brain to learn and memorize data.[189,198] Learning and memorizing are mostly influenced by long-term potentiation (LTP) of the biological synapse, so emulating these functions of biological nerves is an important ability.[214,215] Therefore, relevant fields have focused on brain-inspired neuromorphic computing, which aims to emulate the learning functionality of a biological brain.

However, nervetronics have a very different function than learning. Application of artificial synapses in nervetronics and neuroprosthetics requires emulation of the short-term plasticity (STP), rapid signal transmission, and fast responses of biological peripheral nerves.[149,216–218] Unlike the brain system which is the core system for learning and memorizing, the peripheral nerves are more likely to be operated in the mechanism of STP. Nonvolatile electrochemical artificial synapses have a relatively slow decay response, so they may not be appropriate for nervetronics.

A preferable strategy is to adopt organic artificial synapses that can implement both STP and LTP.[169,200] Moreover, spike-dependent plasticity of artificial synapses gives them the ability to emulate biological synaptic functions. For example, the spike information can be distinguished by rate, number, and duration.

This distinction enables recognition of sensory intensity, or control of movement intensity with nervetronics that use artificial synapses.[31,158,169] These natural mimicry properties of artificial synapses enable event-driven activity and can be the key properties for the biomimetic operation of neuroprosthetics by analog signals.[219] Although application of nervetronics that include artificial synapse for neuroprosthetics is currently in early stages, these promising advantages of nervetronics would fulfill the requirements of next-generation neuroprosthetics.

4.2. Requirements for Neuroprosthetics

Neuroprosthetic devices that use complex CMOS processing units may not be suitable for patients to wear in daily life, because the units are rigid, consume considerable energy, and can decrease the user's satisfaction in life.[220,221] Furthermore, as form of output signals from the CMOS processing units are simple compared to biological nervous signals, which can be incompatible with signaling to a living body,[222–224] signals can be modified to have gradual and biomimicking spike form. But this approach would require additional electrical parts and encoding/decoding of signals, and thus increase the system's complexity and power requirement.[225,226] Consequently, considering the necessity to emulate the natural signal patterns of biological nerves, the complexity of the conventional neuroprosthetics will increase greatly as the number of functions of the nervetronics increase, so this complexification is impractical. So far, studies related to the neuroprosthetics have recovered only very limited motions and senses of limbs such as swing control of the knee joint,[8,22] force control of fingers,[154,156] pressure recognition from limbs,[227] and angle/speed recognition of limbs.[228]

Currently, methods to map the signals from non-biomimetic neuroprosthetics are inadequate and not intuitive, even to adapt to non-biomimetic neuroprosthetics that undergo only simple motions (e.g., single swing and force control).[154,156] However, the human body can control motions such as flexion–extension, abduction–adduction, internal–external rotation, plantar flexion–dorsiflexion, and eversion–inversion[229] and feel stimuli such as pressure, stretch, velocity, vibration, and acceleration in countless ways. Apparently, as the complexity of recovered functions increases, the brain and nervous system may have difficulty in processing signals from the current non-biomimetic CMOS-driven neuroprosthetics.[230] Although the conventional non-biomimetic neuroprosthetics might still work as their complexity of sensorimotor functionality increases, the processes of learning the massive and complex information in each degree of freedom of movement and sensory functions may constitute an overwhelming task for amputees and SCI patients. Thus, biomimetic signals that are natural and intuitive can reduce the processing complexity of the learning and mapping processes.

Therefore, neuromorphic electronic devices that operate with biomimetic signals and provide biological neural actions with synaptic plasticity can provide a breakthrough in the field of neuroprosthetics. To achieve such natural and intuitive neuroprosthetics for everyday use, several requirements must be overcome without degrading the user's quality of life. For example, exoskeletons are currently the most likely candidates to compensate for motor disorders such as amyotrophic lateral

sclerosis, Parkinson's disease, and SCI. However, the suits are bulk and uncomfortable, so they cause injuries such as ankle swelling and chafing (e.g., partial thickness skin loss).[221] These effects can degrade the quality of life of patients. The ideal neuroprosthetics for neurological disease should: 1) emulate the biological neural signal patterns and plasticity, 2) be portable and consume low energy, and 3) be wearable or implantable.

4.2.1. Emulating Biological Nervous Properties

Damage to a component of a neurological path in a biological nervous system can lead to disastrous results because the connection of the path is important. For instance, the premotor cortex (PM) is interconnected with the primary motor cortex (M1), and the M1 has important connections with the primary somatosensory cortex (S1).[231,232] Therefore, damage to the M1 can lead to impaired motor function and limb immobilization by disrupting corticocortical communication among M1, S1, and PM. This disruption results in the disjunction of the corticospinal communication from PM to M1. One attempt to solve this problem is to bypass of M1 by directly connecting PM to S1.

To link distant locations in the cortex, a rigid CMOS-driven Neurochip has been used (**Figure 13**a). It recorded and stimulated the cortical signals of freely moving primates.[19] It creates artificial connections between two sites of the cortex by recording action potentials in one site and triggering electrical stimulation in another site. The Neurochip was programmed to deliver a single stimulus pulse to the stimulation electrode 5 ms after every action potential was detected at the recording electrode. By connecting two distant sites, the Neurochip can create a relationship between them and induce synaptic plasticity mediated by basic synaptic-plasticity mechanism of the biological nervous system (Figure 13b). This artificial connection can replace damaged pathways of the cortex by assisting in formation of connections between two regions.

Similarly, organic nervetronics can couple disconnected nerve cells, but without programming of stimulation signals.[219] Three-terminal artificial synapses with PANI as an active layer and PEO–LiClO$_4$ as a solid electrolyte have been used to couple two completely irrelevant neuron cells. Originally two neuron cells from L5/6 neocortical pyramidal cell in rat brain slice were not coupled, so the activation of Cell 1 did not affected Cell 2 (Figure 13c,d). After the cells were connected to an artificial synapse by using a patch clamp, the action potential from Cell 1 gradually activated Cell 2 (Figure 13e). This gradual rather than immediate activation of Cell 2 is a consequence of the activity-dependent synaptic property of the artificial synapses. Similarly, even though suprathreshold depolarizing step induced an action potential in Cell 1, the artificial synapse that had initial low conductivity evoked subthreshold voltages in Cell 2 ("Before coupling" in Figure 13e). However, as the action potentials from Cell 1 continued, the conductivity of the artificial synapses increased and thereby gradually increased output voltage of artificial synapses and resulted in depolarization of Cell 2 when the voltage reached the action potential threshold ("After coupling" in Figure 13e). Beginning at the 113th spike, Cell 2 started to fire action potentials. Furthermore, as the delivery of spikes continued, the probability

of Cell 2 emitting a spike increased, and the delay in release of an action potential from Cell 2 decreased. This activity-dependent coupling between neurons is the first step in circumventing the injured part of the nervous system.

Organic artificial synapses intrinsically have spike-dependent plasticity, which is very profitable to achieve activity-dependent characteristics.[31,158,169,200] Without the emulation of the synaptic plasticity it needs filters, offset-nulling circuits, analog-to-digital converters, discriminators, and microprocessors that run spike-discrimination algorithms.[220] Although this system can also couple distant neuron cells, the stimulation is only triggered when the neural signal meets the detection criterion, and the pulse is stimulated by the fixed pre-programmed algorithm. However, by emulating biological synaptic plasticity, such complex systems and procedures can be minimized. The artificial synapse alone can implement activity-dependent behaviors, such as "controlling depolarization probability" and "controlling depolarization delay,"[219] so the signals can be applied directly to post-injury nerves to simulate the pre-injury nervous activity. For this reason, artificial synapses that can emulate biological action-potential patterns and plasticity are promising candidates for core systems in next-generation neuroprosthetics.

4.2.2. Low Energy Consumption and Portability

Low energy consumption by neuroprosthetics is an important property to ensure that patients can use them in daily life. Conventional CMOS-driven neuroprosthetics demand excessive energy. Organic artificial synapses that consume energy as low as ≈1.23 fJ per spike event have been reported.[31] Furthermore, activity-dependent behaviors of artificial synapse are more compatible with low energy consumption than conventional CMOS-driven systems. Organic neuroprosthetics consume energy only during input events, and therefore have higher energy efficiency than CMOS-driven systems, which expend standby power to periodically read every pixel. For example, organic systems operate by only using 1/100 of energy when 1% of pixels unlike silicon circuits (**Figure 14**a). Furthermore, the integrated nervetronic system (pressure sensor, ring oscillator, and artificial synapse) only consume ≈8–≈24 μW, calculated using the duty cycle (Figure 14b), due to inherently low energy consuming artificial synapses which only use 0.6 nW–1.2 μW. Use of low-power systems as a component of the neuroprosthetics reduce their power usage.[31]

A flexible artificial nervous system that uses organic materials is more favorable for use in portable and low power neuroprosthetics than is a rigid system that uses silicon-based CMOS. An artificial nervous system composed of organic artificial synapses and organic artificial neurons with a 256-pixel resistive pressure sensor array consumes an estimated 6.5 mW (Figure 14b,c). In contrast, a silicon system with 16 × 16 1T-1R sensor arrays, which consists of decoder, analog multiplexer, current-to-voltage converter, analog-to-digital converter, digital-to-analog converter, and control chip, consumes an estimated 928 mW. This amount is about 143 times larger than that of artificial nervous system.[31,233]

To further increase the portability of the artificial nervous system, an artificial mechanoreceptor was integrated with an
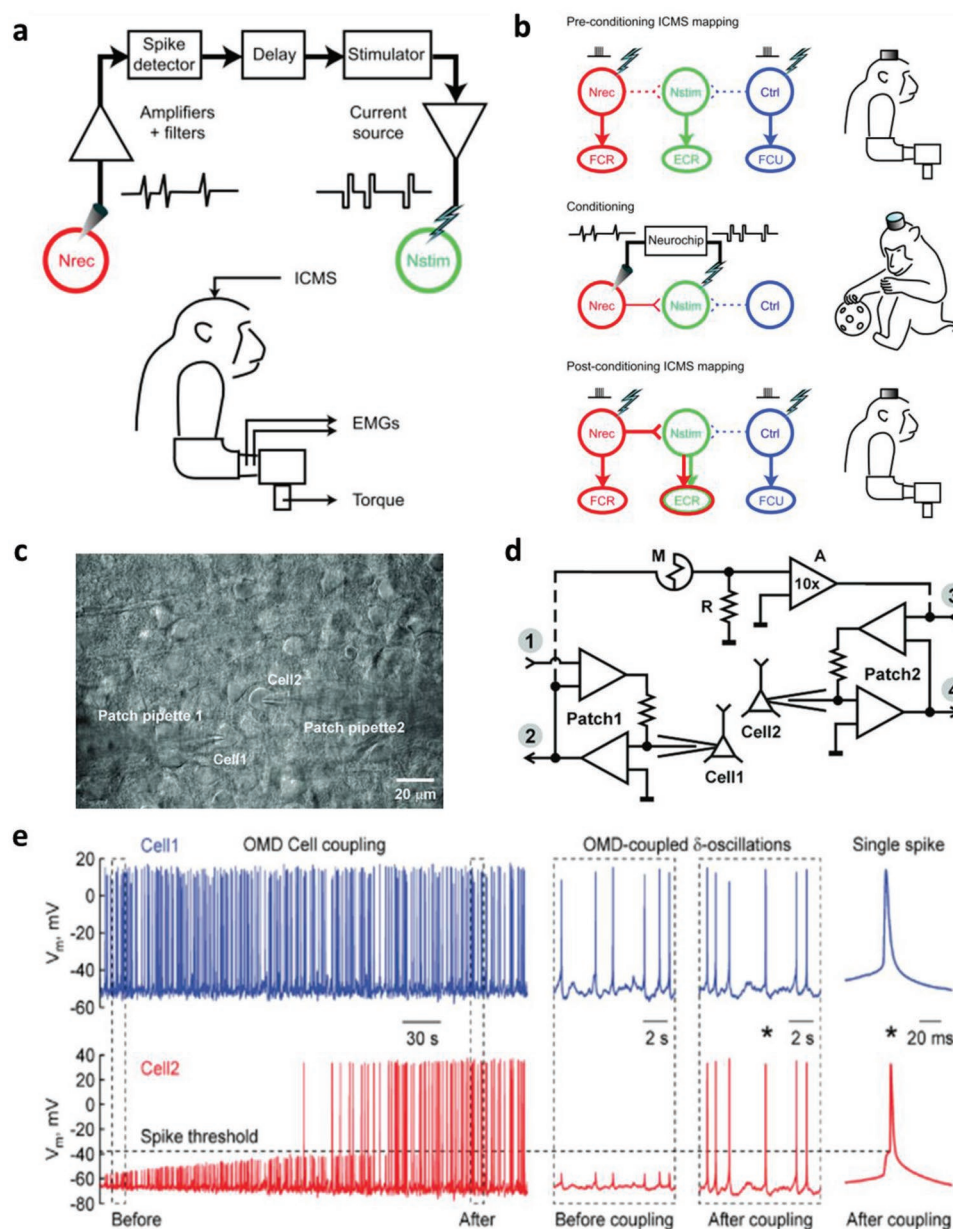
Figure 13. Schematics of artificial connection of neurochips in primate primary motor cortex. a,b) The conditioning protocol of artificial connection (a) and the mechanism of the artificial connection (b). The strengthening of the connection between Nrec and Nstim during the conditioning results in the horizontal projection of activation to Nstim. a,b) Reproduced with permission.[19] Copyright 2006, Springer Nature. c) Microphotography of neo-cortical cells in a rat brain slice. d) Circuit scheme of artificial synapses connecting two separate neuron cells. e) Electrophysiological recording form Cell 1 (blue) and Cell 2 (red). Dashed box: before and after coupling through artificial synapses shown on expanded time scale. The horizontal dashed line indicates the spike threshold of Cell 2. c–e) Reproduced with permission.[219] Copyright 2019, Wiley-VCH.

artificial synaptic transistor to form a simplified single device. By patterning the ion-gel dielectric of the artificial synaptic transistors in a pyramid pattern, the two parts of the artificial nervous system (pressure sensor and artificial synapse) were integrated into a single device.[167] Also, an organic synaptic transistor with ferroelectric polymer dielectric (poly(vinylidene fluoride-trifluoroethylene)) and barium titanate nanoparticles can mimic the slow-adaptive type-I mechanoreceptors in a single device.[186] The low energy consumption of nervetronics, and the ongoing development of strategies to increase portability, will eventually

make organic nervetronics suitable for use by neural-disorder patients without degrading their quality of life.

4.2.3. Wearable and Implantable

Although wearable and implantable systems to treat neurological disorders have been commercialized, the systems are rigid and uncomfortable, so they are not suitable for daily usage. Organic soft materials have outstanding mechanical flexibility,
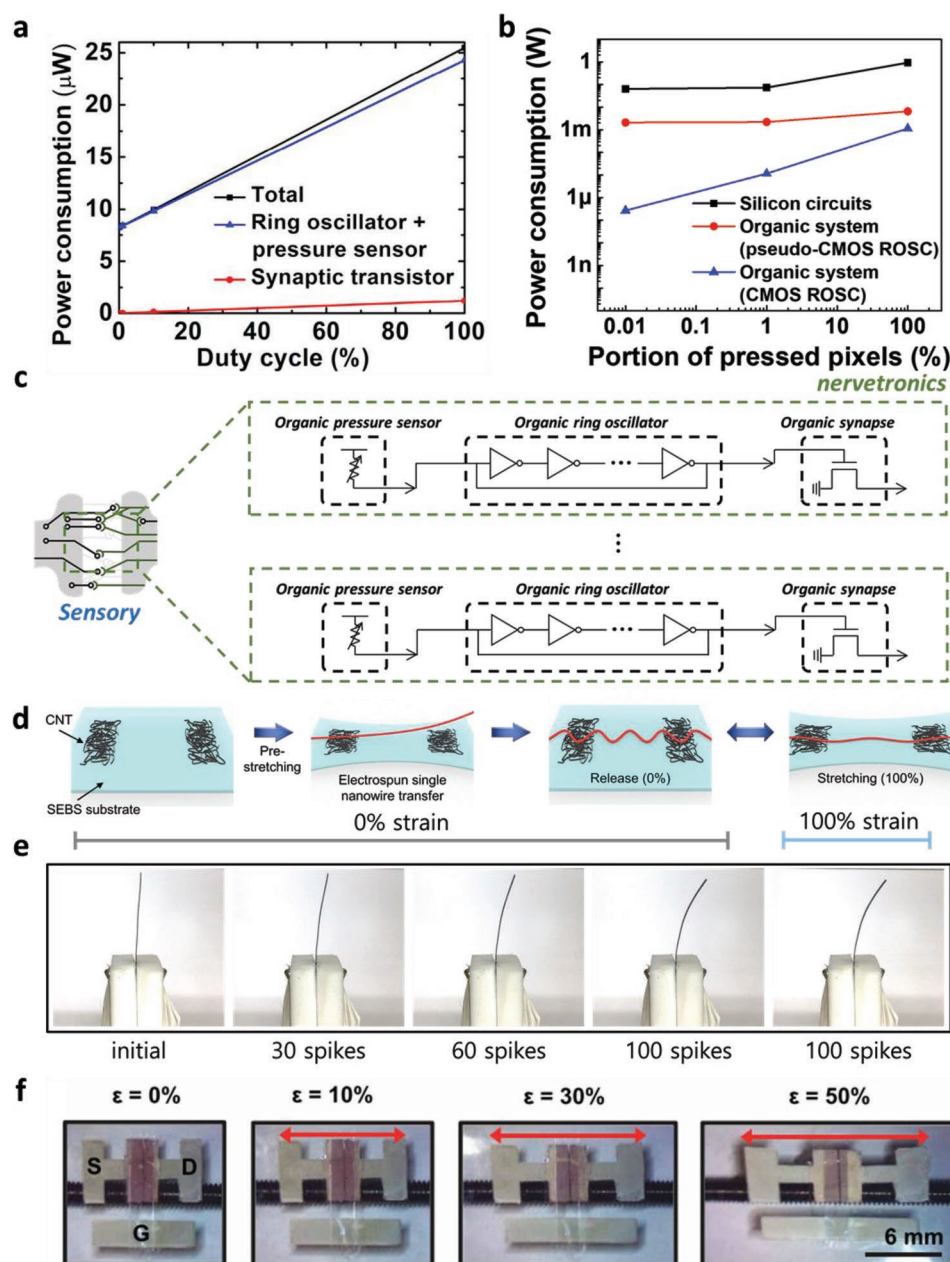
Figure 14. a) Energy efficiency of nervetronics of each part and total system as a function of duty cycle. Reproduced with permission.[31] Copyright 2018, The Authors, published by AAAS. b) Comparison of energy efficiency of silicon circuits (black), nervetronics with pseudo-CMOS ring oscillators (red), and nervetronics with CMOS ring oscillators (blue). Reproduced with permission.[233] Copyright 2021, Elsevier. c) Circuit diagram of the sensory nervetronics with ring oscillator and pressure sensor. In the diagram, the nervetronic circuit has its own output line for each pixel of pressure sensor. d) Schematics stretchable nanowire artificial synapses. e) Digital image of artificial muscle actuator according to 0–100 spikes with 0% strain and 100% strain. c–e) Reproduced with permission.[158] Copyright 2018, The Authors, published by AAAS. From ref. [158]. © The Authors, some rights reserved; exclusive licensee AAAS. Distributed under a CC BY-NC 4.0 license http://creativecommons.org/licenses/by-nc/4.0/. Reprinted with permission from AAAS. f) Photography of intrinsically stretchable artificial synapse. Reproduced with permission.[170] Copyright 2019, The Authors, published by AAAS. From ref. [170]. © The Authors, some rights reserved; exclusive licensee AAAS. Distributed under a CC BY-NC 4.0 license http://creativecommons.org/licenses/by-nc/4.0/. Reprinted with permission from AAAS.

stretchability, and biocompatibility, so organic nervetronics are promising for next generation wearable and implantable neuroprosthetics.

Artificial synapses with wavy ONW semiconductors have been developed to have stable synaptic characteristics without

noticeable degradation upon 100% strain (Figure 14d).[158,241] The single electrospun ONW was transferred onto 100% pre-strained styrene–ethylene–butylene–styrene rubbery substrate. The spike-dependent synaptic properties did not show noticeable change upon strain; therefore, this artificial nervous

**ADVANCED
SCIENCE NEWS**

www.advancedsciencenews.com

**ADVANCED
MATERIALS**

www.advmat.de

system is reliable. Further, the ONW artificial synapse was integrated with a polymer actuator and the combination showed confirmed applicability as a neuroprosthesis. The biomimetic synaptic responses of the artificial synapse controlled the actuator in a biomimetic way without any need for a complex circuit such as a discriminator or microprocessor (Figure 14e). This ability cannot be achieved using conventional single FETs, which usually execute binary outputs (ON, OFF) without multistate short-term or long-term memory response. Due to synaptic potentiation response, the polymer actuator was controlled by input spikes. This activity-dependent behavior of the nervetronics resulted in biomimetic movement of the actuator.

Stretchable artificial synapses have been fabricated using polymer semiconductor nanofibrils in a stretchable polymer matrix (Figure 14f).[170] Fully rubbery synaptic transistors made of poly(3-hexylthiophene) nanofibrils (P3HT-NF) in PDMS, and elastic ion-gel gate dielectric, showed synaptic characteristics upon mechanical stretching by 50%. Due to the stretchability and softness of the device, this fully rubbery transistor array had a low elastic modulus close to that of biological tissue.

The stretchability and softness of the organic materials will enable next-generation wearable and implantable neuroprosthetics without mechanical mismatch with soft tissues. This strategy can realize daily use of neuroprosthetics.

4.3. Progress of Organic Nervetronics for Neuroprosthetics

Ideally, neuroprosthetics should emulate natural patterns of neuronal activity, so that stimulation can be natural and intuitive.[230]

Unlike the conventional neuroprosthetics that do not use a principle of neuroplasticity,[8,20–22,154,156,228] organic nervetronics emulate the neural plasticity of biological nervous system and accomplish low-power, wearable, and implantable neuroprosthetics. Recently, numerous organic artificial afferent and efferent nerves have been demonstrated by integrating artificial neurons and synapses with artificial sensory receptors and artificial muscles.[31,158,164–173] Furthermore, nervetronics have been integrated with living animals.[31,241] Such approaches may facilitate use of organic nervetronics as a core element of neuroprosthetics.

Artificial synapses can emulate biological synaptic functions, so nervetronics can be used to substitute for abnormal biological sensorimotor functions. Nervetronics can implement sensory and motor function of biological counterparts with sensors and actuators by connecting them with artificial synapses and neurons (**Figure 15**a).[31,158,241] Similar to the biological sensory-reception mechanism, the nervetronic system receives sensory information via bioinspired sensory receptors (Figure 15b).[31,149,216] The artificial synapses are spike-dependently activated, so pre-synaptic signals encoded as series of spikes from artificial receptors would be preferred, otherwise signal-converting units would be necessary to transform signals.

A nervetronic device that responds to acoustic signals has been demonstrated by combining artificial synaptic transistors with a triboelectric nanogenerator.[169] Instead of LTP properties that could induce overlap and interfere with high-frequency acoustic signals, STP properties in which the synaptic weight decays within a few milliseconds were demonstrated. This rapid decay reduces temporal overlap of information while retaining
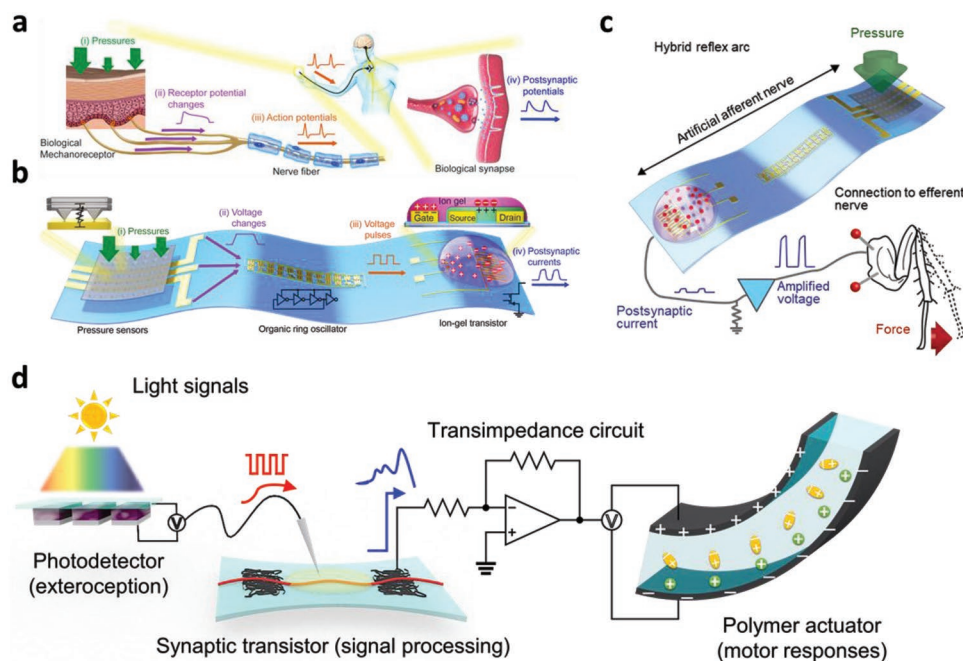

Figure 15. a–c) Schematics of biological afferent nerves (a), nervetronic artificial afferent nerves (b), and hybrid reflex arch (c) demonstrated through connection of biological organ and nervetronics. a–c) Reproduced with permission.[31] Copyright 2018, The Authors, published by AAAS. d) Configuration of artificial efferent nerves attained by integrating nervetronics integrated with an artificial muscle actuator. Reproduced with permission.[158] Copyright 2018, The Authors, published by AAAS. From ref. [158]. © The Authors, some rights reserved; exclusive licensee AAAS. Distributed under a CC BY-NC 4.0 license http://creativecommons.org/licenses/by-nc/4.0/. Reprinted with permission from AAAS.

potentiation of the signals. To achieve STP-dominant properties of the artificial synaptic transistors, the microstructure of the organic semiconducting (OSC) film was controlled.

Artificial synapses composed of polymer semiconductor film have longer retention time in highly crystalline film than in weakly crystalline film.[200] Control of the crystallinity of PTIIG-NP in artificial synapses could adjust their synaptic properties gradually from STP-dominant to LTP-dominant. In EGT-based artificial synapses, the ions penetrate into the polymer semiconducting film when pre-synaptic spikes are applied to the gate electrode.[191,211,213] The penetrated ions are more strongly bound in crystalline regions of the OSC thin films than in their amorphous regions.[200] Consequently, the weakly crystalline film shows STP-dominant synaptic properties and is more suited than highly crystalline film to be used to integrate sensors such as triboelectric nanogenerator for acoustic-signal-responsive nervetronics.[169]

An artificial mechanosensory nerve was developed using artificial synapses composed of diketopyrrolopyrrole (DPP), combined with a pyramidal resistive pressure sensor and artificial neuron.[31] The decay time of these artificial synapses was 2–3 ms, which is comparable to that of biological mechanosensory (slow adaptive-I) nerves (1.5–5 ms).[217,218] The pressure sensor was designed to detect pressure range from 0 to 100 kPa, which is similar to the detection range of the biological mechanoreceptor.[234] The artificial neuron converted continuous signals from the pressure sensor to spike signals. The frequency and the peak voltage of the spike signals were dependent on the input pressure strength. Moreover, signals from multiple pressure sensors were integrated by artificial synapses. The discrete pressure information from six individual pressure sensors was integrated in the artificial synapse, in a manner that is similar to the work of a neuron soma. Finally, the artificial afferent nerves were connected to the leg of an insect to form a hybrid reflex arc (Figure 15c). The leg extended depending on the pressure input; this result demonstrates the feasibility of the nervetronics as neuroprosthetics.

Moreover, artificial efferent nerves that can control muscle movement have been attained using nervetronics (Figure 15d).[158] A conventional functional electrical stimulator (FES) generally uses a constant amplitude of stimulation (up to 120 mA), which can drastically contract the muscle and might cause discomfort.[222] Also, precisely predicting the movement and force of the patient's limbs is challenging.[222–224,226] So, the strategy of ramping the stimulation amplitude during onset and deactivation is commonly used in neuromuscular electrical stimulations to prevent pain or tissue stretch, but this requires an additional procedure for the FES. This additional procedure increases the energy consumption of neuroprosthetics, so patients can be reluctant to use them in daily life. In contrast, the artificial efferent nerves can control the muscle movements precisely because artificial synapses inherently present ramping stimulation as a consequence of the synaptic potentiation responses.[158,241] By connecting not only artificial muscle[158] but also biological muscle[241] with the artificial efferent nerves, the movement of the artificial muscles was controlled in a biomimetic way. This approach can be applied to both arms and legs of amputees and SCI patients and may yield natural and comfortable neuroprosthetics.

5. Conclusion and Outlook

We have considered organic neuroelectronics, including neural interfaces and nervetronics. Organic neuroelectronics are mechanically and electrically compatible with soft biological tissues, so organic neural interfaces and biological nerves can seamlessly exchange electrophysiological signals. The stretchability and non-toxic biocompatibility of organic materials make their neuroelectronic applications wearable and implantable; these traits are difficult to achieve using conventional rigid neuroelectronic devices. Furthermore, the high energy efficiency of organic neuroelectronics would enable them to be highly portable and to operate for long durations. Organic neuroelectronics present a promising approach to future neural interfaces and neuroprosthetics.

Organic materials (CPs, hydrogel composites) and composites of organic materials and carbon allotropes meet a wide range of requirements (e.g., non-toxicity, high capacitance with ionic-electric mixed conduction, mechanical softness, chemical robustness, electrochemical stability, and conformal contact with cells) for use of future in vivo neural interfaces. Especially, soft organic neural interfaces have high charge capacity and tissue-like low elastic modulus that make them appropriate for long-term implantable neuroelectrodes. Therefore, various approaches such as adding dopants and physical/chemical treatments of the surface have been evaluated as ways to improve these properties.[63,83,84] However, challenges remain, such as finding ways to increase mechanical and chemical stability, and to prevent adsorption of proteins and biofouling of organic neural interfaces.[67]

CPs that have mechanical conformal contact with tissues and high volumetric capacitance advance the electrophysiological signal recording in EEG, ECoG, ECG, and EMG over the conventional metal electrodes, without causing side effects such as foreign-body effect and glial-cell formation.[17,117] The low impedance and high charge capacity of electrochemical electrodes, permit biological-signal recording with high SNR. Moreover, the OECTs and IGTs have a localized amplification, so they can detect signals with enhanced SNR.[136–139,142–145] The high current density of organic neural interfaces can efficiently deliver stimulation signals to biological tissues and trigger large movement of limbs with use of a low voltage.[106,147] A high-density organic neural interface array patterned on a large area can map the spatiotemporal propagation of signals at single-cell resolution,[144] and this ability can contribute to increasing the precision of the analysis of neural activities and facilitate diagnosis of neural diseases.

Neuroprosthetics with organic neuromorphic synaptic devices (i.e., nervetronics) would enable the functional replacement of damaged biosystems.[31,158,169,241] Important progress of organic nervetronics involves artificial afferent and efferent nerves to replace damaged peripheral nerves and be used in bionic applications. These efforts will accelerate the development of next-generation neuroprosthetics that can be portable, energy-efficient, and implantable. Neuronal closed-loop feedback, which is one of the challenging neuromorphic functions for nervetronics, would enable a real-time feedback loop to autonomously regulate neural interfacing activities of neuroprosthetics by sensing the state of the patient and environment.[20,154,235]

Combination of soft organic neural interfaces, energy-efficient artificial synapses, and analog circuits can accomplish biomimetic neuroprosthetics that operate with analog-like signals and can minimize the need for energy-inefficient and rigid digital circuits that use CMOS. Also, artificial synapses can be further customized to have synaptic responses that completely match the electrophysiological signals of neuron cells. Moreover, spike-rate-dependent and spike-amplitude-dependent responses of artificial synapses can provide bandpass and noise filtering of neural signals;[186,236–240] this ability would further simplify circuit configuration and reduce the power requirement. Therefore, organic neuroelectronics are a possible solution to enable next-generation organic biomedical electronics and neuroprosthetics that are portable, energy-efficient, stretchable, and implantable.

Conflict of Interest

The authors declare no conflict of interest.

[1] GBD 2016 Neurology Collaborators, *Lancet Neurol.* **2019**, *18*, 459.
[2] O. T. Hall, R. P. McGrath, M. D. Peterson, E. H. Chadd, M. J. DeVivo, A. W. Heinemann, C. Z. Kalpakjian, *Arch. Phys. Med. Rehabil.* **2019**, *100*, 95.
[3] M. Simonato, J. Bennett, N. M. Boulis, M. G. Castro, D. J. Fink, W. F. Goins, S. J. Gray, P. R. Lowenstein, L. H. Vandenberghe, T. J. Wilson, J. H. Wolfe, J. C. Glorioso, *Nat. Rev. Neurol.* **2013**, *9*, 277.
[4] D. B. Rubin, H. H. Danish, A. B. Ali, K. Li, S. Larose, A. D. Monk, D. J. Cote, L. Spendley, A. H. Kim, M. S. Robertson, M. Torre, T. R. Smith, S. Izzy, C. A. Jacobson, J. W. Lee, H. Vaitkevicius, *Brain* **2019**, *142*, 1334.
[5] C. Hinderer, N. Katz, E. L. Buza, C. Dyer, T. Goode, P. Bell, L. K. Richman, J. M. Wilson, *Hum. Gene Ther.* **2018**, *29*, 285.
[6] L. McWhirter, A. Carson, J. Stone, *Brain* **2015**, *138*, 1113.
[7] C. Krishnan, L. Santos, M. D. Peterson, M. Ehinger, *Brain Stimul.* **2015**, *8*, 76.
[8] F. B. Wagner, J.-B. Mignardot, C. G. Le Goff-Mignardot, R. Demesmaeker, S. Komi, M. Capogrosso, A. Rowald, I. Seáñez, M. Caban, E. Pirondini, M. Vat, L. A. McCracken, R. Heimgartner, I. Fodor, A. Watrin, P. Seguin, E. Paoles, K. Van Den Keybus, G. Eberle, B. Schurch, E. Pralong, F. Becce, J. Prior, N. Buse, R. Buschman, E. Neufeld, N. Kuster, S. Carda, J. von Zitzewitz, V. Delattre, *Nature* **2018**, *563*, 65.
[9] N. Obidin, F. Tasnim, C. Dagdeviren, *Adv. Mater.* **2020**, *32*, 1901482.
[10] S. Kim, R. Bhandari, M. Klein, S. Negi, L. Rieth, P. Tathireddy, M. Toepper, H. Oppermann, F. Solzbacher, *Biomed. Microdevices* **2009**, *11*, 453.
[11] G. Hong, C. M. Lieber, *Nat. Rev. Neurosci.* **2019**, *20*, 330.
[12] P. Jayakar, J. Gotman, A. S. Harvey, A. Palmini, L. Tassi, D. Schomer, F. Dubeau, F. Bartolomei, A. Yu, P. Kršek, D. Velis, P. Kahane, *Epilepsia* **2016**, *57*, 1735.
[13] J. K. Krauss, N. Lipsman, T. Aziz, A. Boutet, P. Brown, J. W. Chang, B. Davidson, W. M. Grill, M. I. Hariz, A. Horn, M. Schulder, A. Mammis, P. A. Tass, J. Volkmann, A. M. Lozano, *Nat. Rev. Neurol.* **2021**, *17*, 75.
[14] S. R. Patel, C. M. Lieber, *Nat. Biotechnol.* **2019**, *37*, 1007.
[15] L. Luan, X. Wei, Z. Zhao, J. J. Siegel, O. Potnis, C. A. Tuppen, S. Lin, S. Kazmi, R. A. Fowler, S. Holloway, A. K. Dunn, R. A. Chitwood, C. Xie, *Sci. Adv.* **2017**, *3*, e1601966.
[16] X. Yang, T. Zhou, T. J. Zwang, G. Hong, Y. Zhao, R. D. Viveros, T. M. Fu, T. Gao, C. M. Lieber, *Nat. Mater.* **2019**, *18*, 510.
[17] Y. Liu, V. R. Feig, Z. Bao, *Adv. Healthcare Mater.* **2021**, *10*, 2001916.
[18] J. H. Koo, J.-K. Song, D.-H. Kim, D. Son, *ACS Mater. Lett.* **2021**, *3*, 1528.
[19] A. Jackson, J. Mavoori, E. E. Fetz, *Nature* **2006**, *444*, 56.
[20] D. J. Guggenmos, M. Azin, S. Barbay, J. D. Mahnken, C. Dunham, P. Mohseni, R. J. Nudo, *Proc. Natl. Acad. Sci. USA* **2013**, *110*, 21177.
[21] R. Van Den Brand, J. Heutschi, Q. Barraud, J. DiGiovanna, K. Bartholdi, M. Huerlimann, L. Friedli, I. Vollenweider, E. M. Moraud, S. Duis, N. Dominici, S. Micera, P. Musienko, G. Courtine, *Science* **2012**, *336*, 1182.
[22] M. Capogrosso, T. Milekovic, D. Borton, F. Wagner, E. M. Moraud, J. B. Mignardot, N. Buse, J. Gandar, Q. Barraud, D. Xing, E. Rey, S. Duis, Y. Jianzhong, W. K. D. Ko, Q. Li, P. Detemple, T. Denison, S. Micera, E. Bezard, J. Bloch, G. Courtine, *Nature* **2016**, *539*, 284.
[23] M. Bonizzato, G. Pidpruzhnykova, J. DiGiovanna, P. Shkorbatova, N. Pavlova, S. Micera, G. Courtine, *Nat. Commun.* **2018**, *9*, 3015.
[24] N. Wenger, E. M. Moraud, J. Gandar, P. Musienko, M. Capogrosso, L. Baud, C. G. Le Goff, Q. Barraud, N. Pavlova, N. Dominici, I. R. Minev, L. Asboth, A. Hirsch, S. Duis, J. Kreider, A. Mortera, O. Haverbeck, S. Kraus, F. Schmitz, J. DiGiovanna, R. van den Brand, J. Bloch, P. Detemple, S. P. Lacour, E. Bézard, S. Micera, G. Courtine, *Nat. Med.* **2016**, *22*, 138.
[25] Y. Fang, X. Li, Y. Fang, *J. Mater. Chem. C* **2015**, *3*, 6424.
[26] R. M. Owens, G. G. Malliaras, *MRS Bull.* **2010**, *35*, 449.
[27] R. Green, M. R. Abidian, *Adv. Mater.* **2015**, *27*, 7620.
[28] D.-G. Seo, G.-T. Go, H.-L. Park, T.-W. Lee, *MRS Bull.* **2021**, *46*, 321.
[29] Y. Lee, T.-W. Lee, *Acc. Chem. Res.* **2019**, *52*, 964.
[30] L. R. Squire, F. E. Bloom, N. C. Spitzer, S. du Lac, A. Ghosh, D. Berg, *Fundamental Neuroscience*, Academic Press, Cambridge, MA, USA **2008**.
[31] Y. Kim, A. Chortos, W. Xu, Y. Liu, J. Y. Oh, D. Son, J. Kang, A. M. Foudeh, C. Zhu, Y. Lee, S. Niu, J. Liu, R. Pfattner, Z. Bao, T.-W. Lee, *Science* **2018**, *360*, 998.

**ADVANCED
SCIENCE NEWS**

www.advancedsciencenews.com

**ADVANCED
MATERIALS**

www.advmat.de

[32] H.-L. Park, Y. Lee, N. Kim, D.-G. Seo, G.-T. Go, T.-W. Lee, *Adv. Mater.* **2020**, *32*, 1903558.

[33] S. M. Wellman, J. R. Eles, K. A. Ludwig, J. P. Seymour, N. J. Michelson, W. E. McFadden, A. L. Vazquez, T. D. Y. Kozai, *Adv. Funct. Mater.* **2018**, *28*, 1701269.

[34] S. P. Lacour, G. Courtine, J. Guck, *Nat. Rev. Mater.* **2016**, *1*, 16063.

[35] J. W. Jeong, G. Shin, S. I. Park, K. J. Yu, L. Xu, J. A. Rogers, *Neuron* **2015**, *86*, 175.

[36] R. Das, F. Moradi, H. Heidari, *IEEE Trans. Biomed. Circuits Syst.* **2020**, *14*, 343.

[37] J. del Valle, X. Navarro, *Interfaces with the Peripheral Nerve for the Control of Neuroprostheses*, Elsevier, New York **2013**.

[38] C. Xie, J. Liu, T. M. Fu, X. Dai, W. Zhou, C. M. Lieber, *Nat. Mater.* **2015**, *14*, 1286.

[39] M. Ferguson, D. Sharma, D. Ross, F. Zhao, *Adv. Healthcare Mater.* **2019**, *8*, 1900558.

[40] P. K. Campbell, K. E. Jones, R. J. Huber, K. W. Horch, R. A. Normann, *IEEE Trans. Biomed. Eng.* **1991**, *38*, 758.

[41] K. D. Wise, J. B. Angell, A. Starr, *IEEE Trans. Biomed. Eng.* **1970**, *BME-17*, 238.

[42] R. Chen, A. Canales, P. Anikeeva, *Nat. Rev. Mater.* **2017**, *2*, 16093.

[43] F. Lotti, F. Ranieri, G. Vadalà, L. Zollo, G. Di Pino, *Front. Neurosci.* **2017**, *11*, 497.

[44] M. D. Ferro, N. A. Melosh, *Adv. Funct. Mater.* **2018**, *28*, 1704335.

[45] A. M. Dymond, *IEEE Trans. Biomed. Eng.* **1976**, *BME-23*, 274.

[46] E. McGlynn, V. Nabaei, E. Ren, G. Galeote-Checa, R. Das, G. Curia, H. Heidari, *Adv. Sci.* **2021**, *8*, 2002693.

[47] H. Yuk, B. Lu, X. Zhao, *Chem. Soc. Rev.* **2019**, *48*, 1642.

[48] V. Sankar, E. P. R. Dieme, J. C. Sanchez, A. Prasad, T. Nishida, *Front. Neuroeng.* **2014**, *7*, 13.

[49] S. F. Cogan, *Annu. Rev. Biomed. Eng.* **2008**, *10*, 275.

[50] C. R. Butson, C. C. McIntyre, *Clin. Neurophysiol.* **2005**, *116*, 2490.

[51] P. F. Grant, M. M. Lowery, *IEEE Trans. Biomed. Eng.* **2010**, *57*, 2386.

[52] M. T. Becker, *AIP Adv.* **2021**, *11*, 065106.

[53] M. Hejazi, W. Tong, M. R. Ibbotson, S. Prawer, D. J. Garrett, *Front. Neurosci.* **2021**, *15*, 658703.

[54] D. J. Garrett, K. Ganesan, A. Stacey, K. Fox, H. Meffin, S. Prawer, *J. Neural Eng.* **2012**, *9*, 016002.

[55] D. R. Merrill, in *Somatosensory Feedback for Neuroprosthetics*, (Ed.: B. Güçlü), Academic Press, Cambridge, MA, USA **2021**, pp. 77–150.

[56] J. T. Mortimer, D. Kaufman, U. Roessmann, *Ann. Biomed. Eng.* **1980**, *8*, 235.

[57] H. Yamato, M. Ohwa, W. Wernet, *J. Electroanal. Chem.* **1995**, *397*, 163.

[58] G. Schiavone, X. Kang, F. Fallegger, J. Gandar, G. Courtine, S. P. Lacour, *Neuron* **2020**, *108*, 238.

[59] S. Cherevko, A. A. Topalov, A. R. Zeradjanin, I. Katsounaros, K. J. J. Mayrhofer, *RSC Adv.* **2013**, *3*, 16516.

[60] N. Rossetti, J. Hagler, P. Kateb, F. Cicoira, *J. Mater. Chem. C* **2021**, *9*, 7243.

[61] P. Ocón, A. B. Cristobal, P. Herrasti, E. Fatas, *Corros. Sci.* **2005**, *47*, 649.

[62] C. Boehler, F. Oberueber, S. Schlabach, T. Stieglitz, M. Asplund, *ACS Appl. Mater. Interfaces* **2017**, *9*, 189.

[63] A. Inoue, H. Yuk, B. Lu, X. Zhao, *Sci. Adv.* **2020**, *6*, eaay539.

[64] X. Cui, D. C. Martin, *Sens. Actuators* **2003**, *89*, 92.

[65] M. Nishizawa, H. Nozaki, H. Kaji, T. Kitazume, N. Kobayashi, T. Ishibashi, T. Abe, *Biomaterials* **2007**, *28*, 1480.

[66] P. Li, K. Greben, R. Wördenweber, U. Simon, A. Offenhäusser, D. Mayer, *RSC Adv.* **2015**, *5*, 39252.

[67] T. D. Y. Kozai, N. B. Langhals, P. R. Patel, X. Deng, H. Zhang, K. L. Smith, J. Lahann, N. A. Kotov, D. R. Kipke, *Nat. Mater.* **2012**, *11*, 1065.

[68] T. D. Y. Kozai, A. S. Jaquins-Gerstl, A. L. Vazquez, A. C. Michael, X. T. Cui, *ACS Chem. Neurosci.* **2015**, *6*, 48.

[69] V. Viswam, M. E. J. Obien, F. Franke, U. Frey, A. Hierlemann, *Front. Neurosci.* **2019**, *13*, 385.

[70] F. He, R. Lycke, M. Ganji, C. Xie, L. Luan, *iScience* **2020**, *23*, 101387.

[71] J. Pas, A. L. Rutz, P. P. Quilichini, A. Slézia, A. Ghestem, A. Kaszas, M. J. Donahue, V. F. Curto, R. P. O'Connor, C. Bernard, A. Williamson, G. G. Malliaras, *J. Neural Eng.* **2018**, *15*, 065001.

[72] F. Vitale, D. G. Vercosa, A. V. Rodriguez, S. S. Pamulapati, F. Seibt, E. Lewis, J. S. Yan, K. Badhiwala, M. Adnan, G. Royer-Carfagni, M. Beierlein, C. Kemere, M. Pasquali, J. T. Robinson, *Nano Lett.* **2018**, *18*, 326.

[73] J. Liu, T. M. Fu, Z. Cheng, G. Hong, T. Zhou, L. Jin, M. Duvvuri, Z. Jiang, P. Kruskal, C. Xie, Z. Suo, Y. Fang, C. M. Lieber, *Nat. Nanotechnol.* **2015**, *10*, 629.

[74] A. Williamson, M. Ferro, P. Leleux, E. Ismailova, A. Kaszas, T. Doublet, P. Quilichini, J. Rivnay, B. Rózsa, G. Katona, C. Bernard, G. G. Malliaras, *Adv. Mater.* **2015**, *27*, 4405.

[75] A. Golabchi, K. M. Woeppel, X. Li, C. F. Lagenaur, X. T. Cui, *Biosens. Bioelectron.* **2020**, *155*, 112096.

[76] K. Namsheer, C. S. Rout, *RSC Adv.* **2021**, *11*, 5659.

[77] P. M. Biesheuvel, Y. Fu, M. Z. Bazant, *Phys. Rev. E* **2011**, *83*, 061507.

[78] K. D. Fong, T. Wang, S. K. Smoukov, *Sustainable Energy Fuels* **2017**, *1*, 1857.

[79] R. Balint, N. J. Cassidy, S. H. Cartmell, *Acta Biomater.* **2014**, *10*, 2341.

[80] D. H. Kim, S. M. Richardson-Burns, J. L. Hendricks, C. Sequera, D. C. Martin, *Adv. Funct. Mater.* **2007**, *17*, 79.

[81] V. Castagnola, E. Descamps, A. Lecestre, L. Dahan, J. Remaud, L. G. Nowak, C. Bergaud, *Biosens. Bioelectron.* **2015**, *67*, 450.

[82] M. R. Abidian, J. M. Corey, D. R. Kipke, D. C. Martin, *Small* **2010**, *6*, 421.

[83] R. A. Green, R. T. Hassarati, L. Bouchinet, C. S. Lee, G. L. M. Cheong, J. F. Yu, C. W. Dodds, G. J. Suaning, L. A. Poole-Warren, N. H. Lovell, *Biomaterials* **2012**, *33*, 5875.

[84] S. Baek, R. A. Green, L. A. Poole-Warren, *J. Biomed. Mater. Res., Part A* **2014**, *102*, 2743.

[85] M. Khorrami, M. R. Abidian, in *2018 40th Annu. Int. Conf. of the IEEE Engineering in Medicine and Biology Society (EMBC)*, IEEE, Piscataway, NJ, USA **2018**, pp. 6080–6083.

[86] B. Xu, J. Pei, L. Feng, X.-D. Zhang, *J. Mater. Chem. B* **2021**, *9*, 9485.

[87] M. Devi, M. Vomero, E. Fuhrer, E. Castagnola, C. Gueli, S. Nimbalkar, M. Hirabayashi, S. Kassegne, T. Stieglitz, S. Sharma, *J. Neural Eng.* **2021**, *18*, 041007.

[88] J. Nam, H. K. Lim, N. H. Kim, J. K. Park, E. S. Kang, Y. T. Kim, C. Heo, O. S. Lee, S. G. Kim, W. S. Yun, M. Suh, Y. H. Kim, *ACS Nano* **2020**, *14*, 664.

[89] E. W. Keefer, B. R. Botterman, M. I. Romero, A. F. Rossi, G. W. Gross, *Nat. Nanotechnol.* **2008**, *3*, 434.

[90] H. N. Schwerdt, E. Zhang, M. J. Kim, T. Yoshida, L. Stanwicks, S. Amemori, H. E. Dagdeviren, R. Langer, M. J. Cima, A. M. Graybiel, *Commun. Biol.* **2018**, *1*, 144.

[91] J. J. Clark, S. G. Sandberg, M. J. Wanat, J. O. Gan, E. A. Horne, A. S. Hart, C. A. Akers, J. G. Parker, I. Willuhn, V. Martinez, S. B. Evans, N. Stella, P. E. M. Phillips, *Nat. Methods* **2010**, *7*, 126.

[92] F. Deku, A. Joshi-Imre, A. Mertiri, T. J. Gardner, S. F. Cogan, *J. Electrochem. Soc.* **2018**, *165*, D375.

[93] M. A. Hejazi, W. Tong, A. Stacey, S. H. Sun, M. Yunzab, A. Almasi, Y. J. Jung, H. Meffin, K. Fox, K. Edalati, A. Nadarajah, S. Prawer, M. R. Ibbotson, D. J. Garrett, *Adv. Funct. Mater.* **2020**, *30*, 2006101.

[94] S. Zhao, X. Liu, Z. Xu, H. Ren, B. Deng, M. Tang, L. Lu, X. Fu, H. Peng, Z. Liu, X. Duan, *Nano Lett.* **2016**, *16*, 7731.

[95] A. Bourrier, P. Shkorbatova, M. Bonizzato, E. Rey, Q. Barraud, G. Courtine, R. Othmen, V. Reita, V. Bouchiat, C. Delacour, *Adv. Healthcare Mater.* **2019**, *8*, 1801331.

[96] F. Vitale, S. R. Summerson, B. Aazhang, C. Kemere, M. Pasquali, *ACS Nano* **2015**, *9*, 4465.

[97] A. Capasso, J. Rodrigues, M. Moschetta, F. Buonocore, G. Faggio, G. Messina, M. J. Kim, J. Kwon, E. Placidi, F. Benfenati, M. Bramini, G. H. Lee, N. Lisi, *Adv. Funct. Mater.* **2021**, *31*, 2005300.

[98] A. G. Zestos, C. B. Jacobs, E. Trikantzopoulos, A. E. Ross, B. J. Venton, *Anal. Chem.* **2014**, *86*, 8568.

[99] N. Behabtu, C. C. Young, D. E. Tsentalovich, O. Kleinerman, X. Wang, A. W. K. Ma, E. A. Bengio, R. F. T. Waarbeek, J. J. De Jong, R. E. Hoogerwerf, S. B. Fairchild, J. B. Ferguson, B. Maruyama, J. Kono, Y. Talmon, Y. Cohen, M. J. Otto, M. Pasquali, *Science* **2013**, *339*, 182.

[100] C. Sung, W. Jeon, K. S. Nam, Y. Kim, H. Butt, S. Park, *J. Mater. Chem. B* **2020**, *8*, 6624.

[101] L. V. Kayser, D. J. Lipomi, *Adv. Mater.* **2019**, *31*, 1806133.

[102] R. D. Pyarasani, T. Jayaramudu, A. John, *J. Mater. Sci.* **2019**, *54*, 974.

[103] Y. Shi, L. Pan, B. Liu, Y. Wang, Y. Cui, Z. Bao, G. Yu, *J. Mater. Chem. A* **2014**, *2*, 6086.

[104] M. Shur, F. Fallegger, E. Pirondini, A. Roux, A. Bichat, Q. Barraud, G. Courtine, S. P. Lacour, *ACS Appl. Bio Mater.* **2020**, *3*, 4388.

[105] B. Lu, H. Yuk, S. Lin, N. Jian, K. Qu, J. Xu, X. Zhao, *Nat. Commun.* **2019**, *10*, 1043.

[106] Y. Liu, J. Liu, S. Chen, T. Lei, Y. Kim, S. Niu, H. Wang, X. Wang, A. M. Foudeh, J. B. H. Tok, Z. Bao, *Nat. Biomed. Eng.* **2019**, *3*, 58.

[107] V. R. Feig, H. Tran, M. Lee, Z. Bao, *Nat. Commun.* **2018**, *9*, 2740.

[108] D. Gan, Z. Huang, X. Wang, L. Jiang, C. Wang, M. Zhu, F. Ren, L. Fang, K. Wang, C. Xie, X. Lu, *Adv. Funct. Mater.* **2020**, *30*, 1907678.

[109] S. Ghosh, O. Inganäs, *Adv. Mater.* **1999**, *11*, 1214.

[110] Y. Wang, Y. Shi, L. Pan, Y. Ding, Y. Zhao, Y. Li, Y. Shi, G. Yu, *Nano Lett.* **2015**, *15*, 7736.

[111] C. Cha, S. R. Shin, N. Annabi, M. R. Dokmeci, A. Khademhosseini, *ACS Nano* **2013**, *7*, 2891.

[112] M. R. Abidian, D. C. Martin, *Adv. Funct. Mater.* **2009**, *19*, 573.

[113] Y. Liang, A. Offenhäusser, S. Ingebrandt, D. Mayer, *Adv. Healthcare Mater.* **2021**, *10*, 2100061.

[114] D. Gao, K. Parida, P. S. Lee, *Adv. Funct. Mater.* **2020**, *30*, 1907184.

[115] R. Biran, D. C. Martin, P. A. Tresco, *Exp. Neurol.* **2005**, *195*, 115.

[116] A. Blau, A. Murr, S. Wolff, E. Sernagor, P. Medini, G. Iurilli, C. Ziegler, F. Benfenati, *Biomaterials* **2011**, *32*, 1778.

[117] R. M. Owens, G. G. Malliaras, *MRS Bull.* **2012**, *35*, 86.

[118] M. Zhang, Z. Tang, X. Liu, J. Van der Spiegel, *Nat. Electron.* **2020**, *3*, 191.

[119] D. Khodagholy, J. N. Gelinas, Z. Zhao, M. Yeh, M. Long, J. D. Greenlee, W. Doyle, O. Devinsky, G. Buzsáki, *Sci. Adv.* **2016**, *2*, e160102.

[120] N. Lago, A. Cester, *Appl. Sci.* **2017**, *7*, 1292.

[121] J. Gonzalez-Martinez, J. Mullin, S. Vadera, J. Bulacio, G. Hughes, S. Jones, R. Enatsu, I. Najm, *J. Neurosurg.* **2014**, *120*, 639.

[122] C. Herff, D. J. Krusienski, P. Kubben, *Front. Neurosci.* **2020**, *14*, 123.

[123] L. Luan, J. T. Robinson, B. Aazhang, T. Chi, K. Yang, X. Li, H. Rathore, A. Singer, S. Yellapantula, Y. Fan, Z. Yu, C. Xie, *Neuron* **2020**, *108*, 302.

[124] M. Ganji, E. Kaestner, J. Hermiz, N. Rogers, A. Tanaka, D. Cleary, S. H. Lee, J. Snider, M. Halgren, G. R. Cosgrove, B. S. Carter, D. Barba, I. Uguz, G. G. Malliaras, S. S. Cash, V. Gilja, E. Halgren, S. A. Dayeh, *Adv. Funct. Mater.* **2018**, *28*, 1700232.

[125] D. Khodagholy, T. Doublet, M. Gurfinkel, P. Quilichini, E. Ismailova, P. Leleux, T. Herve, S. Sanaur, C. Bernard, G. G. Malliaras, *Adv. Mater.* **2011**, *23*, H268.

[126] D. Khodagholy, J. N. Gelinas, T. Thesen, W. Doyle, O. Devinsky, G. G. Malliaras, G. Buzsáki, *Nat. Neurosci.* **2015**, *18*, 310.

[127] D. Qi, Z. Liu, Y. Liu, Y. Jiang, W. R. Leow, M. Pal, S. Pan, H. Yang, Y. Wang, X. Zhang, J. Yu, B. Li, Z. Yu, W. Wang, X. Chen, *Adv. Mater.* **2017**, *29*, 1702800.

[128] L. M. Ferrari, U. Ismailov, J.-M. Badier, F. Greco, E. Ismailova, *npj Flexible Electron.* **2020**, *4*, 4.

[129] P. Tallgren, S. Vanhatalo, K. Kaila, J. Voipio, *Clin. Neurophysiol.* **2005**, *116*, 799.

[130] T. C. Ferree, P. Luu, G. S. Russell, D. M. Tucker, *Clin. Neurophysiol.* **2001**, *112*, 536.

[131] Y. M. Chi, T. P. Jung, G. Cauwenberghs, *IEEE Rev. Biomed. Eng.* **2010**, *3*, 106.

[132] A. Searle, L. Kirkup, *Physiol. Meas.* **2000**, *21*, 271.

[133] D. Kim, J. A. Wiler, D. J. Anderson, D. R. Kipke, D. C. Martin, *Acta Biomater.* **2010**, *6*, 57.

[134] S. Oribe, S. Yoshida, S. Kusama, S. Osawa, A. Nakagawa, M. Iwasaki, T. Tominaga, M. Nishizawa, *Sci. Rep.* **2019**, *9*, 13379.

[135] G. D. Spyropoulos, J. Savarin, E. F. Gomez, D. T. Simon, M. Berggren, J. N. Gelinas, E. Stavrinidou, D. Khodagholy, *Adv. Mater. Technol.* **2020**, *5*, 1900652.

[136] D. Khodagholy, T. Doublet, P. Quilichini, M. Gurfinkel, P. Leleux, A. Ghestem, E. Ismailova, T. Hervé, S. Sanaur, C. Bernard, G. G. Malliaras, *Nat. Commun.* **2013**, *4*, 1575.

[137] S. Chen, A. Surendran, X. Wu, S. Y. Lee, M. Stephen, W. L. Leong, *Adv. Mater. Technol.* **2020**, *5*, 2000523.

[138] Y. Liang, M. Ernst, F. Brings, D. Kireev, V. Maybeck, A. Offenhäusser, D. Mayer, *Adv. Healthcare Mater.* **2018**, *7*, 1800304.

[139] L. Bai, C. G. Elósegui, W. Li, P. Yu, J. Fei, L. Mao, *Front. Chem.* **2019**, *7*, 313.

[140] C. M. Proctor, J. Rivnay, G. G. Malliaras, *J. Polym. Sci., Part B: Polym. Phys.* **2016**, *54*, 1433.

[141] J. Rivnay, P. Leleux, M. Ferro, M. Sessolo, A. Williamson, D. A. Koutsouras, D. Khodagholy, M. Ramuz, X. Strakosas, R. M. Owens, C. Benar, J.-M. Badier, C. Bernard, G. G. Malliaras, *Sci. Adv.* **2015**, *1*, e1400251.

[142] G. D. Spyropoulos, J. N. Gelinas, D. Khodagholy, *Sci. Adv.* **2019**, *5*, eaau7378.

[143] C. Cea, G. D. Spyropoulos, P. Jastrzebska-Perfect, J. J. Ferrero, J. N. Gelinas, D. Khodagholy, *Nat. Mater.* **2020**, *19*, 679.

[144] J. Liu, X. Zhang, Y. Liu, M. Rodrigo, P. D. Loftus, J. Aparicio-Valenzuela, J. Zheng, T. Pong, K. J. Cyr, M. Babakhanian, J. Hasi, J. Li, Y. Jiang, C. J. Kenney, P. J. Wang, A. M. Lee, Z. Bao, *Proc. Natl. Acad. Sci. USA* **2020**, *117*, 14769.

[145] W. Lee, S. Kobayashi, M. Nagase, Y. Jimbo, I. Saito, Y. Inoue, T. Yambe, M. Sekino, G. G. Malliaras, T. Yokota, M. Tanaka, T. Someya, *Sci. Adv.* **2018**, *4*, eaau2426.

[146] K. Sim, F. Ershad, Y. Zhang, P. Yang, H. Shim, Z. Rao, Y. Lu, A. Thukral, A. Elgalad, Y. Xi, B. Tian, D. A. Taylor, C. Yu, *Nat. Electron.* **2020**, *3*, 775.

[147] S. Zhao, P. Tseng, J. Grasman, Y. Wang, W. Li, B. Napier, B. Yavuz, Y. Chen, L. Howell, J. Rincon, F. G. Omenetto, D. L. Kaplan, *Adv. Mater.* **2018**, *30*, 1800598.

[148] Y. Liu, J. Li, S. Song, J. Kang, Y. Tsao, S. Chen, V. Mottini, K. McConnell, W. Xu, Y.-Q. Zheng, J. B. H. Tok, P. M. George, Z. Bao, *Nat. Biotechnol.* **2020**, *38*, 1031.

[149] B. C. K. Tee, A. Chortos, A. Berndt, A. K. Nguyen, A. Tom, A. McGuire, Z. C. Lin, K. Tien, W. G. Bae, H. Wang, P. Mei, H. H. Chou, B. Cui, K. Deisseroth, T. N. Ng, Z. Bao, *Science* **2015**, *350*, 313.

[150] K. Deisseroth, *Nat. Methods* **2011**, *8*, 26.

[151] W. Lee, D. Kim, J. Rivnay, N. Matsuhisa, T. Lonjaret, T. Yokota, H. Yawo, M. Sekino, G. G. Malliaras, T. Someya, *Adv. Mater.* **2016**, *28*, 9722.

[152] W. Lee, D. Kim, N. Matsuhisa, M. Nagase, M. Sekino, G. G. Malliaras, T. Yokota, T. Someya, *Proc. Natl. Acad. Sci. USA* **2017**, *114*, 10554.

[153] D. Kim, T. Yokota, T. Suzuki, S. Lee, T. Woo, W. Yukita, M. Koizumi, Y. Tachibana, H. Yawo, H. Onodera, M. Sekino, T. Someya, *Proc. Natl. Acad. Sci. USA* **2020**, *117*, 21138.

**ADVANCED
SCIENCE NEWS**

www.advancedsciencenews.com

**ADVANCED
MATERIALS**

www.advmat.de

[154] E. D'Anna, G. Valle, A. Mazzoni, I. Strauss, F. Iberite, J. Patton, F. M. Petrini, S. Raspopovic, G. Granata, R. Di Iorio, M. Controzzi, C. Cipriani, T. Stieglitz, P. M. Rossini, S. Micera, *Sci. Rob.* **2019**, *4*, eaau8892.

[155] S. Raspopovic, *Science* **2020**, *370*, 290.

[156] S. Raspopovic, M. Capogrosso, F. M. Petrini, M. Bonizzato, J. Rigosa, G. Di Pino, J. Carpaneto, M. Controzzi, T. Boretius, E. Fernandez, G. Granata, C. M. Oddo, L. Citi, A. L. Ciancio, C. Cipriani, M. C. Carrozza, W. Jensen, E. Guglielmelli, T. Stieglitz, P. M. Rossini, S. Micera, *Sci. Transl. Med.* **2014**, *6*, 222ra19.

[157] D. Borton, S. Micera, J. D. R. Millán, G. Courtine, *Sci. Transl. Med.* **2013**, *5*, 210rv2.

[158] Y. Lee, J. Y. Oh, W. Xu, O. Kim, T. R. Kim, J. Kang, Y. Kim, D. Son, J. B.-H. Tok, M. J. Park, Z. Bao, T.-W. Lee, *Sci. Adv.* **2018**, *4*, eaat7387.

[159] A. L. Benabid, *Curr. Opin. Neurobiol.* **2003**, *13*, 696.

[160] J. S. Perlmutter, J. W. Mink, *Annu. Rev. Neurosci.* **2006**, *29*, 229.

[161] M. L. Kringelbach, N. Jenkinson, S. L. F. Owen, T. Z. Aziz, *Nat. Rev. Neurosci.* **2007**, *8*, 623.

[162] J. Caylor, R. Reddy, S. Yin, C. Cui, M. Huang, C. Huang, R. Rao, D. G. Baker, A. Simmons, D. Souza, S. Narouze, R. Vallejo, I. Lerman, *Bioelectron. Med.* **2019**, *5*, 12.

[163] G. Barolat, *Arch. Med. Res.* **2000**, *31*, 258.

[164] C. Wan, G. Chen, Y. Fu, M. Wang, N. Matsuhisa, S. Pan, L. Pan, H. Yang, Q. Wan, L. Zhu, X. Chen, *Adv. Mater.* **2018**, *30*, 1801291.

[165] D. Choi, M. K. Song, T. Sung, S. Jang, J. Y. Kwon, *Nano Energy* **2020**, *74*, 104912.

[166] X. Yang, J. Yu, J. Zhao, Y. Chen, G. Gao, Y. Wang, Q. Sun, Z. L. Wang, *Adv. Funct. Mater.* **2020**, *30*, 2002506.

[167] D. W. Kim, J. C. Yang, S. Lee, S. Park, *ACS Appl. Mater. Interfaces* **2020**, *12*, 23207.

[168] X. Zhang, Y. Zhuo, Q. Luo, Z. Wu, R. Midya, Z. Wang, W. Song, R. Wang, N. K. Upadhyay, Y. Fang, F. Kiani, M. Rao, Y. Yang, Q. Xia, Q. Liu, M. Liu, J. J. Yang, *Nat. Commun.* **2020**, *11*, 51.

[169] D.-G. Seo, Y. Lee, G.-T. Go, M. Pei, S. Jung, Y. H. Jeong, W. Lee, H.-L. Park, S.-W. Kim, H. Yang, C. Yang, T.-W. Lee, *Nano Energy* **2019**, *65*, 104035.

[170] H. Shim, K. Sim, F. Ershad, P. Yang, A. Thukral, Z. Rao, H.-J. Kim, Y. Liu, X. Wang, G. Gu, L. Gao, X. Wang, Y. Chai, C. Yu, *Sci. Adv.* **2019**, *5*, eaax4961.

[171] C. Wan, P. Cai, X. Guo, M. Wang, N. Matsuhisa, L. Yang, Z. Lv, Y. Luo, X. J. Loh, X. Chen, *Nat. Commun.* **2020**, *11*, 4602.

[172] J. Yu, G. Gao, J. Huang, X. Yang, J. Han, H. Zhang, Y. Chen, C. Zhao, Q. Sun, Z. L. Wang, *Nat. Commun.* **2021**, *12*, 1581.

[173] H. R. Lee, D. Lee, J. H. Oh, *Adv. Mater.* **2021**, *33*, 2100119.

[174] L. Fang, S. Dai, Y. Zhao, D. Liu, J. Huang, *Adv. Electron. Mater.* **2020**, *6*, 1901217.

[175] M. Yang, X. Zhao, Q. Tang, N. Cui, Z. Wang, Y. Tong, Y. Liu, *Nanoscale* **2018**, *10*, 18135.

[176] Y. Park, J. S. Lee, *ACS Nano* **2017**, *11*, 8962.

[177] M.-K. Kim, J.-S. Lee, *ACS Appl. Mater. Interfaces* **2018**, *10*, 10280.

[178] N. Raeis-Hosseini, J.-S. Lee, *ACS Appl. Mater. Interfaces* **2016**, *8*, 7326.

[179] N. R. Hosseini, J. S. Lee, *Adv. Funct. Mater.* **2015**, *25*, 5586.

[180] S.-R. Zhang, L. Zhou, J.-Y. Mao, Y. Ren, J.-Q. Yang, G.-H. Yang, X. Zhu, S.-T. Han, V. A. L. Roy, Y. Zhou, *Adv. Mater. Technol.* **2019**, *4*, 1800342.

[181] M. K. Choi, W. K. Kim, S. Sung, C. Wu, H. W. Kim, T. W. Kim, *Sci. Rep.* **2018**, *8*, 12275.

[182] L. Tu, S. Yuan, J. Xu, K. Yang, P. Wang, X. Cui, X. Zhang, J. Wang, Y.-Q. Zhan, L.-R. Zheng, *RSC Adv.* **2018**, *8*, 26549.

[183] W. Xu, T. L. Nguyen, Y. T. Kim, C. Wolf, R. Pfattner, J. Lopez, B.-G. Chae, S.-I. Kim, M. Y. Lee, E.-Y. Shin, Y.-Y. Noh, J. H. Oh, H. Hwang, C.-G. Park, H. Y. Woo, T.-W. Lee, *Nano Energy* **2018**, *48*, 575.

[184] T. Fu, X. Liu, H. Gao, J. E. Ward, X. Liu, B. Yin, Z. Wang, Y. Zhuo, D. J. F. Walker, J. J. Yang, J. Chen, D. R. Lovley, J. Yao, *Nat. Commun.* **2020**, *11*, 1861.

[185] H.-L. Park, T.-W. Lee, *Org. Electron.* **2021**, *98*, 106301.

[186] Y. R. Lee, T. Q. Trung, B. U. Hwang, N. E. Lee, *Nat. Commun.* **2020**, *11*, 2753.

[187] A. Melianas, T. J. Quill, G. LeCroy, Y. Tuchman, H. V. Loo, S. T. Keene, A. Giovannitti, H. R. Lee, I. P. Maria, I. McCulloch, A. Salleo, *Sci. Adv.* **2020**, *6*, eabb2958.

[188] P. Gkoupidenis, N. Schaefer, X. Strakosas, J. A. Fairfield, G. G. Malliaras, *Appl. Phys. Lett.* **2015**, *107*, 263302.

[189] E. J. Fuller, S. T. Keene, A. Melianas, Z. Wang, S. Agarwal, Y. Li, Y. Tuchman, C. D. James, M. J. Marinella, J. J. Yang, A. Salleo, A. A. Talin, *Science* **2019**, *364*, 570.

[190] P. Gkoupidenis, D. A. Koutsouras, T. Lonjaret, J. A. Fairfield, G. G. Malliaras, *Sci. Rep.* **2016**, *6*, 27007.

[191] W. Xu, S.-Y. Min, H. Hwang, T.-W. Lee, *Sci. Adv.* **2016**, *2*, e1501326.

[192] S. Ham, M. Kang, S. Jang, J. Jang, S. Choi, T. W. Kim, G. Wang, *Sci. Adv.* **2020**, *6*, eaba1178.

[193] P. Gkoupidenis, N. Schaefer, B. Garlan, G. G. Malliaras, *Adv. Mater.* **2015**, *27*, 7176.

[194] P. Gkoupidenis, D. A. Koutsouras, G. G. Malliaras, *Nat. Commun.* **2017**, *8*, 15448.

[195] S. T. Keene, A. Melianas, Y. van de Burgt, A. Salleo, *Adv. Electron. Mater.* **2018**, *0*, 1800686.

[196] L. Kong, J. Sun, C. Qian, J. Fu, J. Wang, J. Yang, Y. Gao, *Org. Electron.* **2017**, *47*, 126.

[197] S. T. Keene, C. Lubrano, S. Kazemzadeh, A. Melianas, Y. Tuchman, G. Polino, P. Scognamiglio, L. Cinà, A. Salleo, Y. van de Burgt, F. Santoro, *Nat. Mater.* **2020**, *19*, 969.

[198] Y. van de Burgt, E. Lubberman, E. J. Fuller, S. T. Keene, G. C. Faria, S. Agarwal, M. J. Marinella, A. A. Talin, A. Salleo, *Nat. Mater.* **2017**, *16*, 414.

[199] S. Jang, S. Jang, E.-H. Lee, M. Kang, G. Wang, T.-W. Kim, *ACS Appl. Mater. Interfaces* **2019**, *11*, 1071.

[200] G.-T. Go, Y. Lee, D.-G. Seo, M. Pei, W. Lee, H. Yang, T.-W. Lee, *Adv. Intell. Syst.* **2020**, *2*, 2000012.

[201] J. Lenz, F. del Giudice, F. R. Geisenhof, F. Winterer, R. T. Weitz, *Nat. Nanotechnol.* **2019**, *14*, 579.

[202] Y. Choi, S. Oh, C. Qian, J. H. Park, J. H. Cho, *Nat. Commun.* **2020**, *11*, 4595.

[203] K.-N. Kim, M.-J. Sung, H.-L. Park, T.-W. Lee, *Adv. Electron. Mater.* **2021**, *8*, 2100935.

[204] M. J. Panzer, C. D. Frisbie, *Adv. Mater.* **2008**, *20*, 3177.

[205] S. H. Kim, K. Hong, W. Xie, K. H. Lee, S. Zhang, T. P. Lodge, C. D. Frisbie, *Adv. Mater.* **2013**, *25*, 1822.

[206] J. Lee, M. J. Panzer, Y. He, T. P. Lodge, C. D. Frisbie, *J. Am. Chem. Soc.* **2007**, *129*, 4532.

[207] M. J. Panzer, C. D. Frisbie, *J. Am. Chem. Soc.* **2007**, *129*, 6599.

[208] Y. Xia, J. Cho, B. Paulsen, C. D. Frisbie, M. J. Renn, *Appl. Phys. Lett.* **2009**, *94*, 013304.

[209] F. Torricelli, D. Z. Adrahtas, Z. Bao, M. Berggren, F. Biscarini, A. Bonfiglio, C. A. Bortolotti, C. D. Frisbie, E. Macchia, G. G. Malliaras, I. McCulloch, M. Moser, T.-Q. Nguyen, R. M. Owens, A. Salleo, A. Spanu, L. Torsi, *Nat. Rev. Methods Primers* **2021**, *1*, 66.

[210] J. T. Friedlein, R. R. McLeod, J. Rivnay, *Org. Electron.* **2018**, *63*, 398.

[211] T. J. Quill, G. LeCroy, A. Melianas, D. Rawlings, Q. Thiburce, R. Sheelamanthula, C. Cheng, Y. Tuchman, S. T. Keene, I. McCulloch, R. A. Segalman, M. L. Chabinyc, A. Salleo, *Adv. Funct. Mater.* **2021**, *31*, 2104301.

[212] D. A. Bernards, G. G. Malliaras, *Adv. Funct. Mater.* **2007**, *17*, 3538.

[213] J. Rivnay, S. Inal, A. Salleo, R. M. Owens, M. Berggren, G. G. Malliaras, *Nat. Rev. Mater.* **2018**, *3*, 17086.

[214] L. F. Abbott, W. G. Regehr, *Nature* **2004**, *431*, 796.
[215] V. M. Ho, J.-A. Lee, K. C. Martin, *Science* **2011**, *334*, 623.
[216] W. W. Lee, Y. J. Tan, H. Yao, S. Li, H. H. See, M. Hon, K. A. Ng, B. Xiong, J. S. Ho, B. C. K. Tee, *Sci. Rob.* **2019**, *4*, eaax2198.
[217] Y. Takeuchi, M. Yamasaki, Y. Nagumo, K. Imoto, M. Watanabe, M. Miyata, *J. Neurosci.* **2012**, *32*, 6917.
[218] F. Bengtsson, R. Brasselet, R. S. Johansson, A. Arleo, H. Jörntell, *PLoS One* **2013**, *8*, e56630.
[219] E. Juzekaeva, A. Nasretdinov, S. Battistoni, T. Berzina, S. Iannotta, R. Khazipov, V. Erokhin, M. Mukhtarov, *Adv. Mater. Technol.* **2019**, *4*, 1800350.
[220] J. Mavoori, A. Jackson, C. Diorio, E. Fetz, *J. Neurosci. Methods* **2005**, *148*, 71.
[221] C. B. Baunsgaard, U. V. Nissen, A. K. Brust, A. Frotzler, C. Ribeill, Y. B. Kalke, N. León, B. Gómez, K. Samuelsson, W. Antepohl, U. Holmström, N. Marklund, T. Glott, A. Opheim, J. Benito, N. Murillo, J. Nachtegaal, W. Faber, F. Biering-Sørensen, *Spinal Cord* **2018**, *56*, 106.
[222] E. L. Nussbaum, P. Houghton, J. Anthony, S. Rennie, B. L. Shay, A. M. Hoens, *Physiother. Can.* **2017**, *69*, 1.
[223] B. M. Doucet, A. Lam, L. Griffin, *Yale J. Biol. Med.* **2012**, *85*, 201.
[224] J. Wang, H. Wang, C. Lee, *Adv. Biosyst.* **2019**, *3*, 1800281.
[225] B. J. Broderick, D. E. O'Briain, P. P. Breen, S. R. Kearns, G. ÓLaighin, *Med. Eng. Phys.* **2010**, *32*, 349.
[226] M. Bijak, M. Rakos, C. Hofer, W. Mayr, M. Strohhofer, D. Raschka, H. Kern, *Artif. Organs* **2005**, *29*, 220.
[227] F. M. Petrini, G. Valle, M. Bumbasirevic, F. Barberi, D. Bortolotti, P. Cvancara, A. Hiairrassary, P. Mijovic, A. Ö. Sverrisson, A. Pedrocchi, J. L. Divoux, I. Popovic, K. Lechler, B. Mijovic, D. Guiraud, T. Stieglitz, A. Alexandersson, S. Micera, A. Lesic, S. Raspopovic, *Sci. Transl. Med.* **2019**, *11*, eaav8939.
[228] F. M. Petrini, M. Bumbasirevic, G. Valle, V. Ilic, P. Mijović, P. Čvančara, F. Barberi, N. Katic, D. Bortolotti, D. Andreu, K. Lechler, A. Lesic, S. Mazic, B. Mijović, D. Guiraud, T. Stieglitz, A. Alexandersson, S. Micera, S. Raspopovic, *Nat. Med.* **2019**, *25*, 1356.
[229] D. S. Pamungkas, W. Caesarendra, H. Soebakti, R. Analia, S. Susanto, *Electronics* **2019**, *8*, 1283.
[230] S. J. Bensmaia, D. J. Tyler, S. Micera, *Nat. Biomed. Eng.* **2020**, https://doi.org/10.1038/s41551-020-00630-8.
[231] R. P. Dum, P. L. Strick, *Physiol. Behav.* **2002**, *77*, 677.
[232] K. M. Friel, S. Barbay, S. B. Frost, E. J. Plautz, D. M. Hutchinson, A. M. Stowe, N. Dancause, E. V. Zoubina, B. M. Quaney, R. J. Nudo, *J. Neurophysiol.* **2005**, *94*, 1312.
[233] Y. Lee, H.-L. Park, Y. Kim, T.-W. Lee, *Joule* **2021**, *5*, 794.
[234] D. R. Lesniak, K. L. Marshall, S. A. Wellnitz, B. A. Jenkins, Y. Baba, M. N. Rasband, G. J. Gerling, E. A. Lumpkin, *eLife* **2014**, *3*, e01488.
[235] N. Wenger, E. M. Moraud, S. Raspopovic, M. Bonizzato, J. DiGiovanna, P. Musienko, M. Morari, S. Micera, G. Courtine, *Sci. Transl. Med.* **2014**, *6*, 255ra133.
[236] L. Q. Zhu, C. J. Wan, L. Q. Guo, Y. Shi, Q. Wan, *Nat. Commun.* **2014**, *5*, 3158.
[237] Y. Liu, J. Zhong, E. Li, H. Yang, X. Wang, D. Lai, H. Chen, T. Guo, *Nano Energy* **2019**, *60*, 377.
[238] D. Liu, Q. Shi, S. Dai, J. Huang, *Small* **2020**, *16*, 1907472.
[239] J. Tang, F. Yuan, X. Shen, Z. Wang, M. Rao, Y. He, Y. Sun, X. Li, W. Zhang, Y. Li, B. Gao, H. Qian, G. Bi, S. Song, J. J. Yang, H. Wu, *Adv. Mater.* **2019**, *31*, 1902761.
[240] Y. He, Y. Yang, S. Nie, R. Liu, Q. Wan, *J. Mater. Chem. C* **2018**, *6*, 5336.
[241] Y. Lee, Y. Liu, D.-G. Seo, J. Y. Oh, Y. Kim, J. Li, J. Kang, J. Kim, J. Mun, A. M. Foudeh, Z. Bao, T.-W. Lee, *Nat. Biomed. Eng.* **2022**, https://doi.org/10.1038/s41551-022-00918-x.

Gyeong-Tak Go is a doctoral candidate in the Department of Materials Science and Engineering at Seoul National University, Republic of Korea. He received his B.S. degree in 2018 from the Department of Materials Science and Engineering at Seoul National University. His research interests include neuromorphic electronics based on artificial synapse devices, and stretchable electronics.
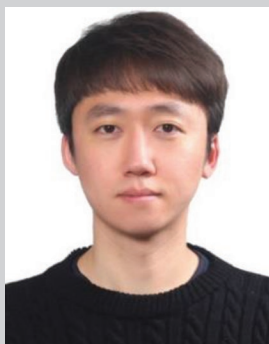
Yeongjun Lee is a postdoctoral researcher in the Department of Chemical Engineering at Stanford University, USA. He received his B.S. in the Department of Materials Science and Engineering (MSE) from Hanyang University, South Korea in 2012. He received his Ph.D. in MSE from Pohang University of Science and Technology (POSTECH), South Korea in 2018. He joined the MSE at Seoul National University, as a postdoctoral researcher and worked at Organic Material Lab at Samsung Advanced Institute of Technology as a staff researcher (2019–2021). His research interests include stretchable electronics, neuromorphic electronics, and bioelectronics.

**ADVANCED
SCIENCE NEWS**
www.advancedsciencenews.com

**ADVANCED
MATERIALS**
www.advmat.de
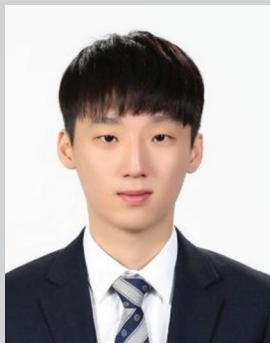
Dae-Gyo Seo is a doctoral candidate in the Department of Materials Science and Engineering at Seoul National University, Republic of Korea. He received his B.S. degree in 2018 from the Department of Materials Science and Engineering from Korea University, Republic of Korea. His research interests include organic transistors, neuromorphic electronics, artificial nerve systems, and biointegration systems.

Tae-Woo Lee is a professor in the Department of MSE at Seoul National University, South Korea. He received his Ph.D. in chemical engineering from KAIST, South Korea in 2002. He joined Bell Laboratories, USA, as a postdoctoral researcher and worked at Samsung Advanced Institute of Technology as a research staff (2003–2008). He was an associate professor in MSE at Pohang University of Science and Technology (POSTECH), South Korea, until August 2016. His research focuses on printed electronics based on organic and organic–inorganic hybrid materials for flexible displays, solid-state lighting, solar energy conversion devices, and bioinspired neuromorphic devices.